iScience

CellPress
OPEN ACCESS

Article

In vitro vascularized immunocompetent patient-derived model to test cancer therapies

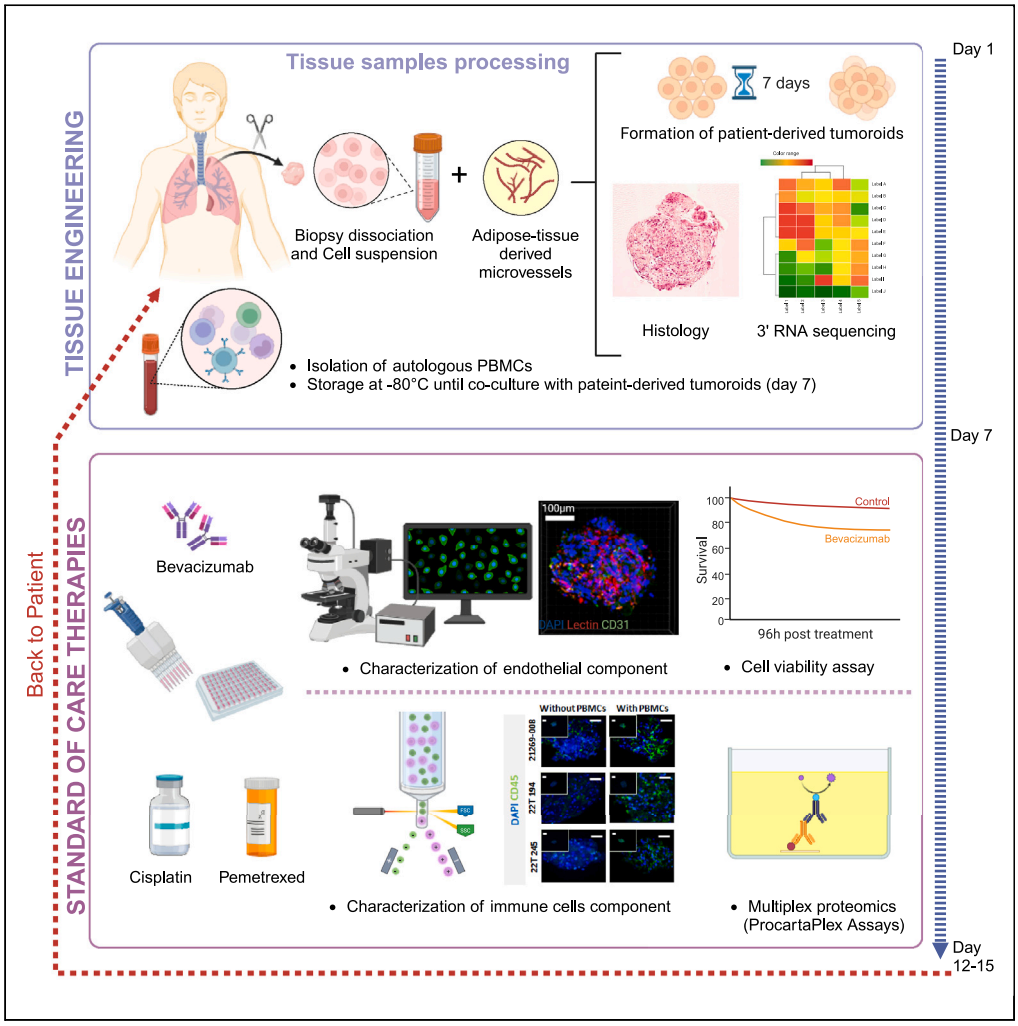

Hélène Lê, Jules Deforges, Guoqiang Hua, ..., Eric Quéméneur, Nadia Benkirane-Jessel, Jean-Marc Balloul

quemeneur@transgene.fr (E.Q.)
nadia.jessel@inserm.fr (N.B.-J.)
balloul@transgene.fr (J.-M.B.)

Highlights

Patients' tumoral cells and heterologous microvessels form vascularized tumoroids

ECM, vascularization, and immune cells are maintained in tumoroid microenvironment

Antiangiogenic treatment effects are reproduced on tumoroids

A combination of cisplatin and pemetrexed shows an immunosuppressive effect

Lê et al., iScience 26, 108094
October 20, 2023 © 2023
https://doi.org/10.1016/j.isci.2023.108094

iScience

CellPress
OPEN ACCESS

Article

In vitro vascularized immunocompetent patient-derived model to test cancer therapies

Hélène Lê,[1,2,5] Jules Deforges,[1] Guoqiang Hua,[2] Ysia Idoux-Gillet,[2] Charlotte Ponté,[2,3] Véronique Lindner,[2] Anne Olland,[2,3] Pierre-Emanuel Falcoz,[2,3] Cécile Zaupa,[4] Shreyansh Jain,[1] Eric Quéméneur,[1,*] Nadia Benkirane-Jessel,[2,*] and Jean-Marc Balloul[1,*]

SUMMARY

This work describes a patient-derived tumoroid model (PDTs) to support precision medicine in lung oncology. The use of human adipose tissue-derived microvasculature and patient-derived peripheral blood mononuclear cells (PBMCs) permits to achieve a physiologically relevant tumor microenvironment. This study involved ten patients at various stages of tumor progression. The vascularized, immune-infiltrated PDT model could be obtained within two weeks, matching the requirements of the therapeutic decision. Histological and transcriptomic analyses confirmed that the main features from the original tumor were reproduced. The 3D tumor model could be used to determine the dynamics of response to antiangiogenic therapy and platinum-based chemotherapy. Antiangiogenic therapy showed a significant decrease in vascular endothelial growth factor (VEGF)-A expression, reflecting its therapeutic effect in the model. In an immune-infiltrated PDT model, chemotherapy showed the ability to decrease the levels of lymphocyte activation gene-3 protein (LAG-3), B and T lymphocyte attenuator (BTLA), and inhibitory receptors of T cells functions.

INTRODUCTION

Lung cancer represents 18% of all cancer deaths.[1] It divides into two subsets: non-small-cell lung cancer (NSCLC) which affects 85% of lung cancer patients and small-cell lung cancer (SCLC), which affects the remaining 15%. Forty percent of NSCLC patients present an adenocarcinoma.[2] Nearly half of NSCLC patients are usually diagnosed at late stages.[3] Consequently, the 5-year relative survival rate remains low, at about 6%, despite the progress of chemotherapy, targeted therapy, or immunotherapy.[4] Currently, the selection of the best treatment for NSCLC is based on three important methods: (i) staging, (ii) histological subtyping, and (iii) molecular profiling. Sixty percent of adenocarcinoma patients display a mutation in driver genes, such as KRAS or EGFR.[5,6] Identifying these mutations has led to the development of tyrosine kinase inhibitors targeting specific mutations (e.g., EGFR, MET, ALK, ROS-1 …). Targeted therapies have helped improve objective responses rate and progression-free survival compared to chemotherapy. However, 60% of patients can develop acquired resistance under the first and second rounds of tyrosine kinases inhibitors, leading to disease progression.[7] As adjuncts of chemotherapy and targeted therapy, immune checkpoint inhibitors (ICIs) have helped to improve patient's survival further. However, less than 30% advanced-stage NSCLC patients are responders to ICIs pembrolizumab as 1st line treatment.[8]

Several approaches have been designed to consider better patient-specific biological characteristics to drive the selection of the best treatment option.[9] In this context, patient-derived tumoroids (PDTs) have been explored mainly for their ability to recapitulate key features of the tumor.[10] However, important tumor-extrinsic factors such as stromal and immune cells have been missing, and the generation of PDTs also involves non-human components, such as murine-based growth factors in Matrigel©.[11–15] In this study, one of our objectives was to represent the tumor complexity by incorporating cells mainly involved in tumoral progression and therapeutic responses. For that purpose, PDTs were generated under scaffold-free conditions, as described by Seitlinger et al.,[16] and in the presence of human pulmonary fibroblasts that were shown at that time to be necessary to form consistent intact PDTs.[16] Cancer-associated fibroblasts (CAFs) have been broadly described in co-culture with tumoral patients' cells,[17] exploiting their role as regulators of the extracellular matrix.[18] However, some limitations were reported for integrating CAFs in the 3D model, particularly functional heterogeneity, strong pro-tumorigenic effects, and high-immunosuppressive effects.[19,20] This might negatively impact the prediction of response to treatment, and we thus explored another approach based on a vascularized PDT model.

[1]Transgene S.A, 400 Boulevard Gonthier d'Andernach, 67400 Illkirch-Graffenstaden, France
[2]INSERM UMR 1260, Regenerative Nanomedicine, 1 rue Eugène Boeckel, 67000 Strasbourg, France
[3]Hopitaux Universitaires de Strasbourg, 1 Place de l'Hôpital, 67000 Strasbourg, France
[4]Boehringer Ingelheim, 29 avenue Tony Garnier, 69007 Lyon, France
[5]Lead contact
*Correspondence: quemeneur@transgene.fr (E.Q.), nadia.jessel@inserm.fr (N.B.-J.), balloul@transgene.fr (J.-M.B.)
https://doi.org/10.1016/j.isci.2023.108094

Vascularization is an essential contributor to the tumoral microenvironment as endothelial cells produce different cytokines and growth factors, which could play a significant role in tumor progression.[21] Furthermore, blood vessels facilitate nutrients, oxygen, and drug delivery to tumors. Microvessels derived from adipose tissue (ad-MVs) were shown to be able to form functional vascular networks.[22] They not only contain intact microvascular fragments, including arteriolar, capillary, and venule segments but also stromal and stem cells.[23] The dynamic interplay between PDTs and ad-MVs is key in the formation and function of human tumor surrogates because the vasculature system largely controls tumor progression or metastasis,[23,24] and at the same time, cancer cells are known to define vasculature remodeling.[25,26]

Histological and transcriptomic studies demonstrated that patients' tumorigenicity and specificity were preserved in our PDT model compared to the parental tumor biopsy. In addition, to better represent the immune component of the tumoral microenvironment (TME), vascularized PDTs were cultured in the presence of patient (autologous) peripheral blood mononuclear cells (PBMCs). We could thus incorporate immune infiltration, trafficking, and potential cytotoxic activity of immune cells as readouts for the 3D tumor model. This report describes the key properties of a vascularized PDT platform supplemented with immune cells. Clinical constraints, including patients' specificity and the short time frame of therapeutical decisions, were taken in the system design.

RESULTS

Preservation of histological markers in vascularized PDTs

Vascularized PDTs were formed from different patient's biopsies by co-culturing 5,000 patient' cells and 5,000 Ad-MVs in ultra-low-attachment plates (see STAR Methods). When patient-derived cells were cultured alone, no intact cells assemblies of PDTs and matched healthy organoids could be generated from the primary tumor or healthy cell components (Figure 1A). With the addition of Ad-MVs, the success rate of culture establishment from lung primary samples is 100%. These supportive cells really have an influence in the 3D formation of PDTs and healthy organoids. The morphological organization of the vascular component within the PDT and in the primary tissue was analyzed with anti-PECAM1/CD31 and UEA I-lectin, which are relevant probes for functional endothelial cells.[27,28] The comparative histological analysis of primary tumor samples and corresponding vascularized PDTs confirmed similar spatial expressions for the two biomarkers (Figure 1B).

Hematoxylin-eosin (H&E) staining demonstrated that vascularized PDTs retain major histological features of the primary tumor tissue. The tumoroid model implemented was also able to reproduce original patient-specific tumor features; for patients 21T 414 and 21T 554, comparable glandular morphology was identified on primary tissue and PDTs' paraffin sections (Figure 2). Similarly, for patient 21T 469, the primary tumoral tissue presented a higher necrotic area. Necrosis is associated with weak hematoxylin staining, and this feature was found in both primary tissue and was well recapitulated in PDT sections for this specific patient (Figure 2). Histological analyses confirmed that these three patients were lung adenocarcinomas (Table S1). Different biomarkers confirmed the general equivalence of primary biopsy and vascularized PDTs, and hence the good overall reliability of the proposed model: TTF-1,[29] cytokeratin-7 (CK-7 or KRT7),[30] and mucin-1 (MUC-1)[30] for lung adenocarcinoma-associated markers and Ki-67 for cell proliferation (Figure 2, See also Figure S1). Besides those typical lung adenocarcinoma-associated markers, we also checked for epithelial to mesenchymal transition markers, such as the expression of vimentin or the loss of E-cadherin.[31] The expression of E-cadherin was observed on both tumoral and normal patient cells, as previously reported.[32] However, the vimentin expression was found to be specific in tumor cells and was observed in both primary tissue and vascularized PDTs (See also Figure S2).

Main markers of the TME were also assessed, particularly the extracellular matrix (ECM) with collagen type IV marker[33] and immune cell infiltration with CD45 marker. Collagen IV and CD45 labeling were observed in both the primary tissue and vascularized PDTs (Figure 2) but with lower CD45 labeling in vascularized PDTs.

Transcriptomic signatures of vascularized PDTs are in line with primary tumor cells

We further performed comparative gene expression profiling to characterize the functional comparability of our PDT model. 3′ RNA sequencing allowed differential analysis of (i) tumor primary cells versus healthy primary cells and (ii) vascularized PDTs versus healthy organoids. The differentially expressed transcripts between the primary tumoral cells and the healthy primary cells are displayed in Figure 3. We chose a list of genes of interest specific to tumorigenicity reported in lung adenocarcinoma for the heatmap generation. Specific lung adenocarcinoma-associated biomarkers TTF-1, CK-7 (or KRT7), and MUC-1, already identified in IHC experiments, were also found at the mRNA level. In addition to MUC-1, we could also find upregulated expression of MUC-21 and MUC-4 in primary tumor cells and matched PDTs compared to primary healthy cells and matched healthy organoids, respectively. MUC-21 mRNA expression has been shown to present high-mutation rates, and MUC-4 is described to play a role in the cell growth signaling pathway of lung adenocarcinoma.[34] More cytokeratin (KRT) family transcripts were overexpressed in the primary tumoral cells or PDTs compared to primary healthy cells or healthy organoids[35] (Figure 3A). Cytokeratins are markers originating from the cytoskeleton of epithelial cells. They have a role in epithelial protection under cellular stress and functions such as motility, signaling, growth, and protein synthesis.[36] While they are expressed in tissues originating from normal organs, they are also often present in those organ-specific tumors. However, they are overexpressed in tumor cells when compared to the healthy cells. For example, among the cytokeratins' family, KRT7, KRT8, and KRT18 are found abundant in carcinomas.[37] In addition, we have also found other cytokeratins' transcripts in patients' primary tumor cells like KRT6A, KRT7, KRT8, KRT15, KRT17, KRT18, and KRTCAP3. KRT6A, KRT17, and KRT18 are overexpressed in NSCLC and are markers to the positive diagnosis of NSCLC' subtypes.[38] Similarly, KRT17 is overexpressed in many tumor's types.[39,40] KRT7 is significantly expressed in lung adenocarcinoma, concomitantly to SLC34A2, MUC1, and NAPSA.[41] This overexpression was also reflected on our PDT model compared to healthy organoids. The mRNA for

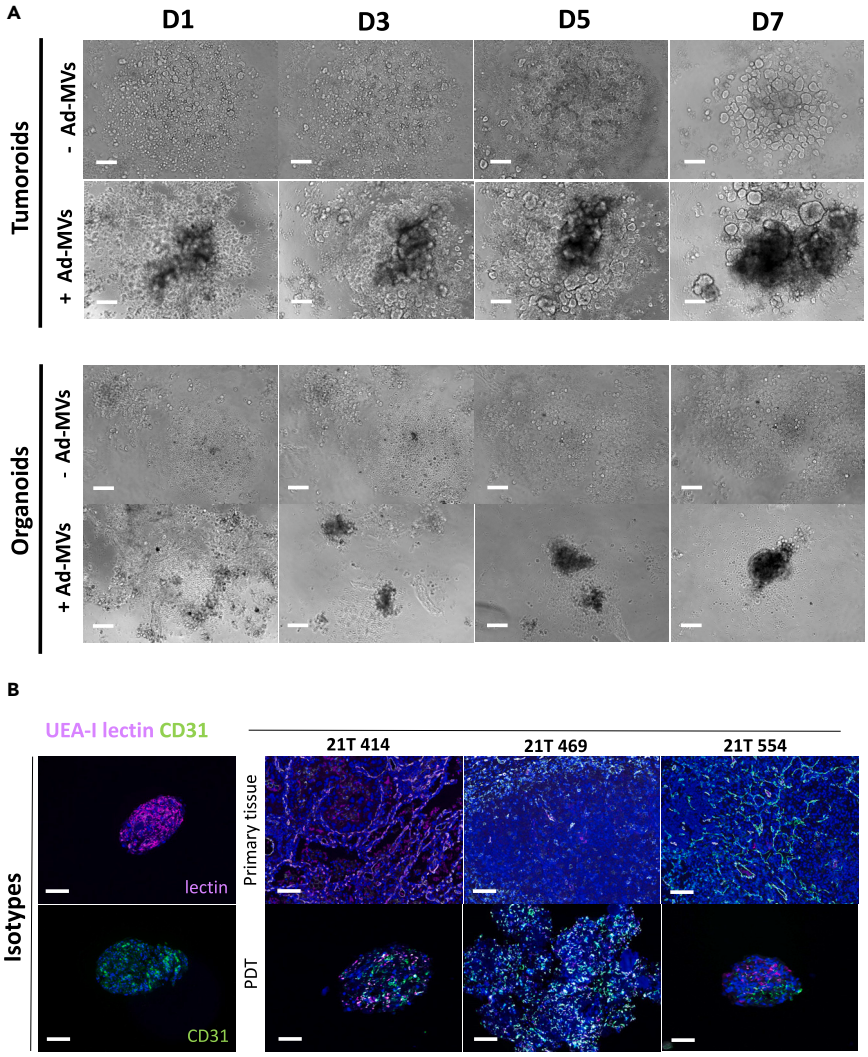

Figure 1. Formation, and organization of patient-derived 3D model

(A) Bright-field images, time-course (day 1 to day 7) analysis of tumoroid, and healthy organoid formation, from either tumor or normal cells derived from patient biopsies, respectively, and in the presence or absence of adipose-derived microvessels (±Ad-MVs).

(B) Comparative IHC staining for vascular biomarkers in 3 patients. Primary tissues were compared to corresponding vascularized PDTs at day 7 of co-culture. Scale bars 100μm.

NAPSA was observed in PDTs in accordance with the tumoral primary cells from patients 21T 414 and 21T 554. S100P mRNA was also overexpressed in tumoral primary tissue and PDTs compared to healthy samples. They were previously observed in lung adenocarcinoma and are involved in tumor development and metastasis.[42] Thus, NAPSA, S100P, and others such as S100A7, S100A14, and S100A9 mRNA, were reported to be significantly upregulated in lung adenocarcinoma.[41] Our PDT model could accurately reproduce this significant upregulation compared to healthy organoids.

The mRNA for epithelial cell adhesion molecule (EPCAM)[43] was upregulated on primary tumoral cells and vascularized PDTs (Figure 3A). Other common genes of tumor development were also maintained during the PDT formation process, such as CEACAM5 and CEACAM6. Noteworthy, CEACAM5 is overexpressed in 20% of NSCLC patients and is now assessed as a therapeutic target for tusamitamab ravtansive (SAR408701), an antibody-drug conjugate currently in phase 3 clinical trial.[44] Regarding the SERPIN transcripts (SERPINA1[45] and SERPINE2[46]), which are involved in pathogenesis of lung cancer, SERPINA1 mRNA could be detected in primary cells and organoids of patient 21T 414 and SERPINE2 mRNA could be detected in patients 21T 554 and 21T 469. Even though their described role in lung pathogenesis, SERPIN transcripts were not overexpressed in tumoral samples compared to healthy samples (Figure 3A). We showed a subset of genes commonly regulated in primary tumoral cells and PDTs.

Altogether, most of these genes related to lung adenocarcinoma were upregulated in not only primary tumoral cells versus primary healthy cells but also in PDT versus healthy organoids.

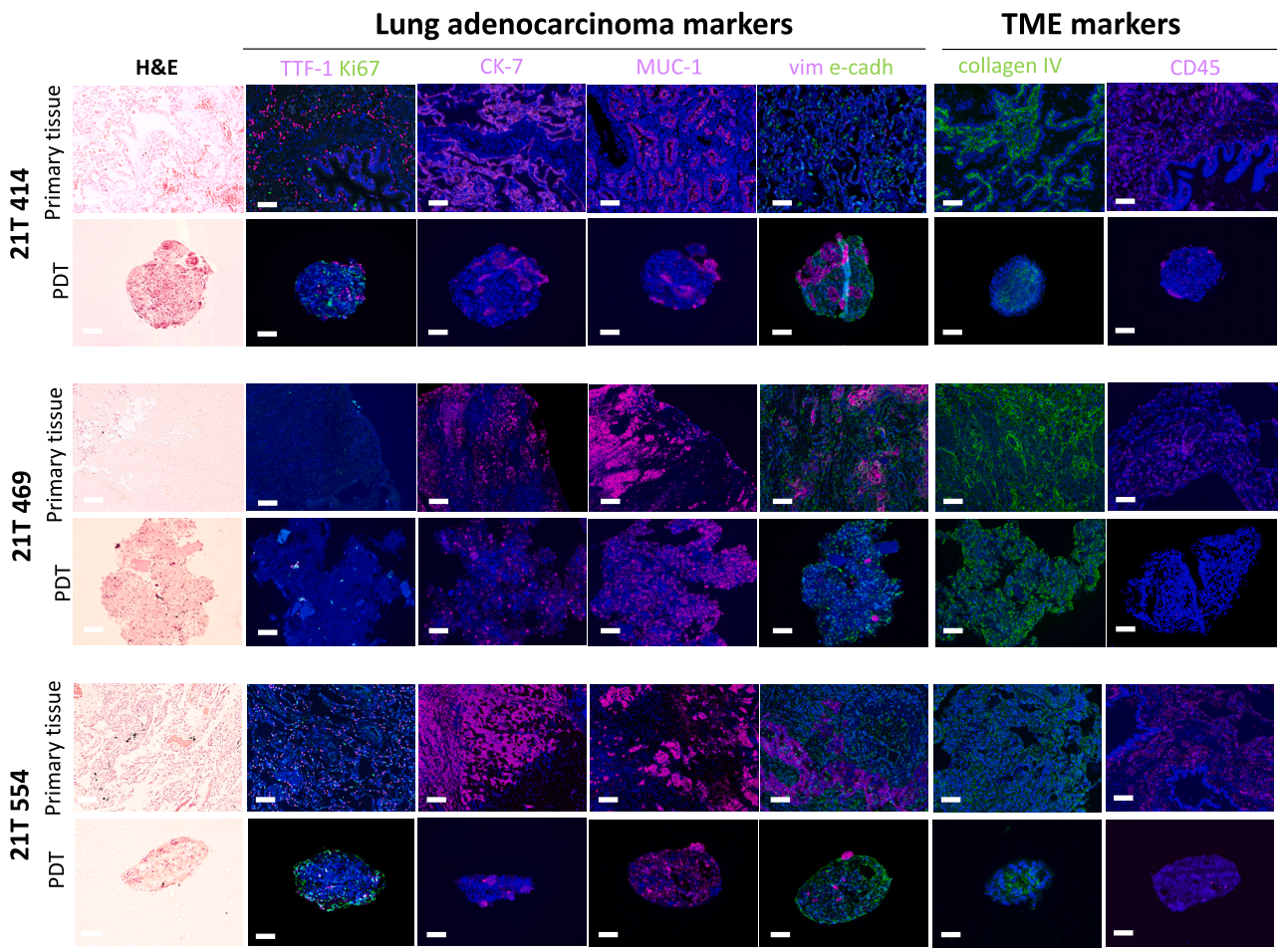

Figure 2. Preservation of histological markers in vascularized PDTs and primary tumor tissue in 3 lung adenocarcinoma patients (21T 414, 21T 469, and 21T 554)

H&E staining of advanced lung cancer primary tissue sections and PDT on the left. IHC staining of lung adenocarcinoma biomarkers with anatomopathologists' routine markers TTF-1, CK-7, and MUC-1. Ki-67 biomarker was used for cell proliferation. Vimentin, biomarker of mesenchymal phenotype and E-cadherin, biomarker of epithelial cells were also assessed to study tumoral progression/invasion state. IHC staining of tumoral microenvironment (TME) biomarkers such as collagen type IV for part of extracellular matrix (ECM) and CD45 for immune cells were studied.

See also Figures S1 and S2.

In addition to these similarities, we still see a positive correlation between genes up or downregulated in primary tumor cells and in PDTs for patient 21T 414 and patient 21T 554. Nearly half of the up and downregulated genes in PDTs for patient 21T 554, and more for patient 21T 414, were found up and downregulated in primary tumor cells compared to primary healthy cells (dark blue and dark red dots in Figure 3B). Certain genes were also found up and downregulated in primary tumor cells but not in the tumoroid model (pink and pale blue dots in Figure 3B).

Taken globally, the transcriptional expression level for all these described genes was similar in primary tumoral tissue and matched PDTs. However, some variabilities were observed in certain patients for the RNA expression, such as TTF-1, which was not detected in tumoral cells for patient 21T 414 but was detected in PDTs. For patient 21T 469, CEACAM6 was not detected in PDTs but in primary tumoral cells. Regarding healthy organoids, they tend to downregulate lung cancer-associated genes compared to tumoroids. This downregulation was also observed in primary healthy cells compared to primary tumor cells (Figure 3A).

Ad-MVs provided a dynamic vascular component to PDTs for assessing the sensitivity to antiangiogenic treatments

Adipose tissue-derived microvessels (Ad-MVs) were previously described as major supportive cells for cell culture,[22,47] by providing different perivascular cells in addition to endothelial cells, in particular smooth muscle cells, mesenchymal stem cells, and other stromal cells.[48]

Their presence in the tumor culture not only supports the formation of intact cellular assemblies but also offers an opportunity to directly assess angiogenic properties *in vitro*[49,50] and the activity of antiangiogenic inhibitors.[51] We studied the typical morphology of Ad-MVs and their ability to enhance some vascular network formation within our PDT model (Figure 4A). On day 7 of the PDTs formation, the vascular

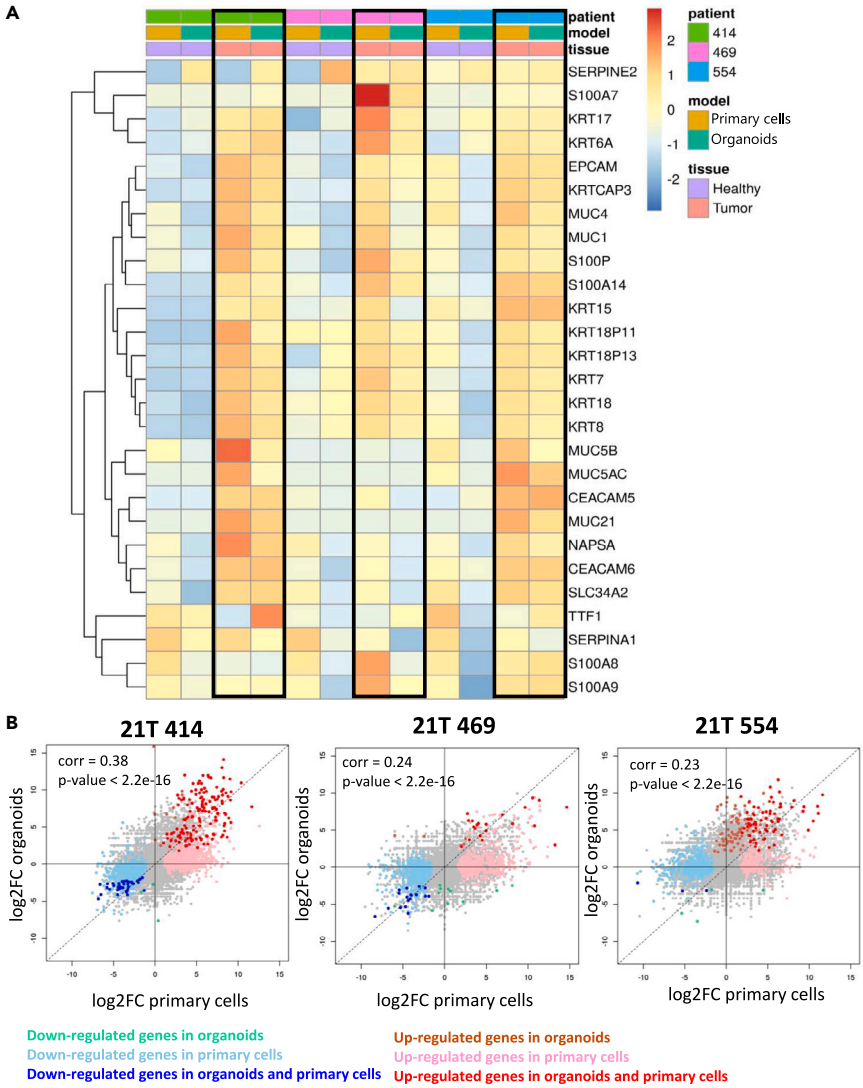

Figure 3. Transcriptomic signatures of vascularized PDTs are in line with primary tumor cells

(A) Heatmap shows the main lung cancer-associated genes that are significantly upregulated in the tumoral primary cells versus healthy primary cells and in the vascularized PDTs versus the healthy organoids according to the 3′ RNA sequencing analysis.

(B) Scatterplot of gene expression analysis as log 2 value. Log2 fold change (l2FC) of mRNA steady-state level for primary tumor cells versus primary healthy cells was plotted (x axis) against log2 fold-change for PDTs versus healthy organoid (y axis). The Pearson correlation coefficient was calculated for each of the three patients independently.

network within the PDTs was characterized with UEA-1 lectin and CD31 staining. Co-localization of both biomarkers is observed, and lumen-like structures could also be observed with confocal microscopy (Figure 4B). The presence of lumen is also confirmed with light-sheet microscopy (See also Figure S3).

On day seven, PDTs were transferred into an insert containing a hydrogel matrix based on a fibrin gel as illustrated, and characterization of endothelial cell structure was done[52] (Figures 4A–4C). The use of matrix or hydrogel provides an *in vitro* approach to develop vascularization, based on physiological processes such as angiogenesis.[53] After 24 h on fibrin gel, some tip cells-like are out of the PDT. This represents the first steps of angiogenesis, from the extension of an endothelial tip cell to forming new vessel branch.[54] CD31 staining and UEA-1 lectin confirmed that these *de novo* structures were made up of endothelial cells[55] (Figure 4C). The projection view in XZ by confocal microscopy further helps to visualize the presence of a lumen (associated with the lectin staining) (Figure 4C).

Starting from forming these *de novo* structures, the antiangiogenic treatment was applied to investigate its antiangiogenic potential. To assess the Ad-MVs dynamic, we applied anti-VEGF or bevacizumab. Antiangiogenic effect was evaluated according to the following criteria: (i) direct blocking of VEGF-A functions, (ii) inhibition or regression of new endothelial cell structures, (iii) alteration of vascular function, and (iv) indirect effects on tumor cells.[56] After 96 h of treatment with bevacizumab *in vitro*, the inhibition and regression of newly formed endothelial

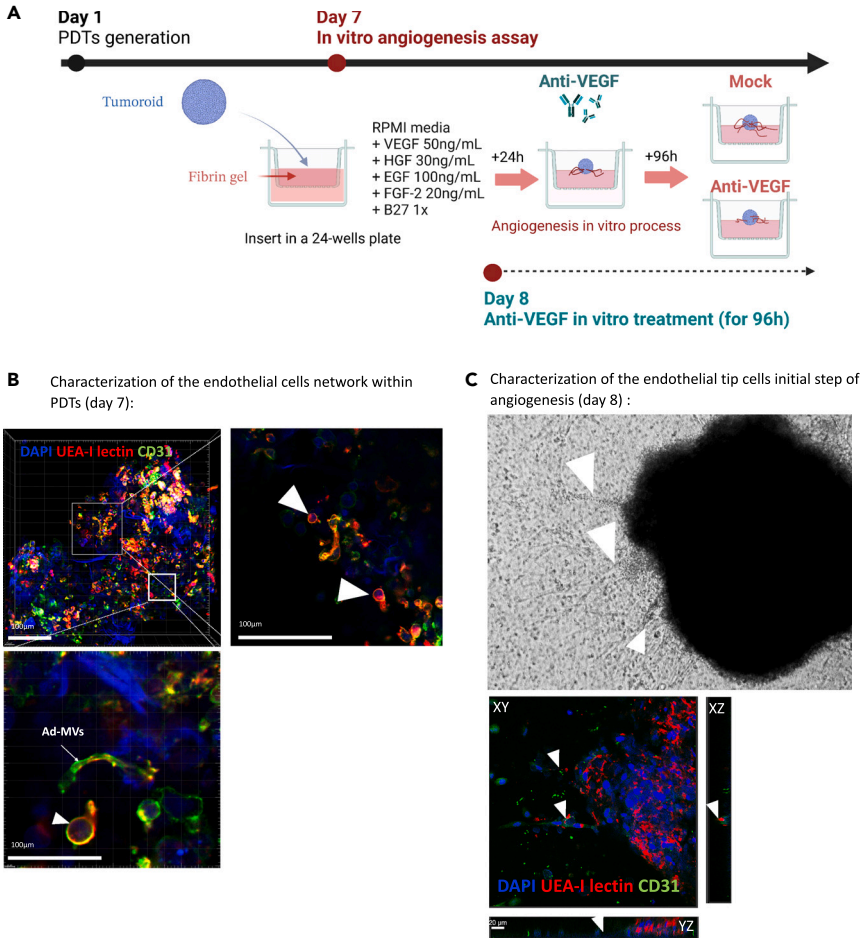

Figure 4. Ad-MVs provided a dynamic vascular component to PDTs for the generation of an *in vitro* anti-angiogenesis assay

(A) Study workflow (vascularized PDTs culture and Anti-VEGF treatment). *In vitro* anti-angiogenesis assay protocol is also detailed.

(B) Confocal images of endothelial cells and Ad-MVs organization within vascularized PDTs on day 7. UEA-I lectin is stained in rhodamine and CD31 is stained in green (5/6-fluorescein isothiocyanate (FITC)). Left image is a 3D view of the PDT in a z-range of 60µm. The two other images (on the right and bottom) were taken at objective ×40, clearly showing the structure of the Ad-MVs with vascular lumen (highlighted by the presence of UEA-I lectin).

(C) Characterization of an endothelial tip cell that was formed 24 h after fibrin gel embedding. (Brightfield contrast photos and by IF). White arrows also show the presence of a vascular lumen with the co-staining of CD31 and UEA-I lectin on the XZ plan.

See also Figure S3.

cell structures were detected, translating into less $CD31^+$ cells surrounding the tumor core (Figure 5A). The quantification of $CD31^+$ cells, based on the mean fluorescence intensity, supported this qualitative observation (Figure 5B). Consequently, the cell viability of PDT, measured via metabolic activity, decreased by about 50% under bevacizumab treatment (Figure 5C). We observed a significant decrease of VEGF-A, the key effector of proliferation and migration of endothelial cells, vascular permeability, and the selection of tip and stalk cells[57] (Figure 5D). Our data confirmed the functional value of our model assay, particularly to study the dynamic role of Ad-MVs in tumoroid physiology and to analyze *in vitro* the impact of antiangiogenic drugs or treatments.

Tri-culture of patients' cells, Ad-MVs, and autologous PBMCs permits to reconstitute a dynamic TME

Lung TME comprises different immune cell populations that actively participate in promotion or regression of lung cancer.[21] Besides infiltration of $CD4^+$ and $CD8^+$ T lymphocytes, the presence of intratumoral B cells is associated with a good prognosis.[21,58,59] A key question was if PDT model could maintain the immune cells from the patient biopsy. We previously showed (Figure 2) that lower levels of immune cells than the original tumor were generally observed in our vascularized PDTs (See also Figures S4 and S5). This observation was also previously reported by other studies.[60] Due to the difficulty of retaining tumor-resident-immune cells over longer time in culture,[61] an alternative approach was implemented in this study to resupply the PDTs with autologous immune cells derived from patient's peripheral blood.[60] The use of autologous PBMCs brings functional relevance to the PDT model because they represent the actual status of circulating immune cells, including naive T cells and tumor-reactive T cells, and they provide a dynamic vision of the TME, in particular for complex processes, such as infiltration and chemotaxis.[62]

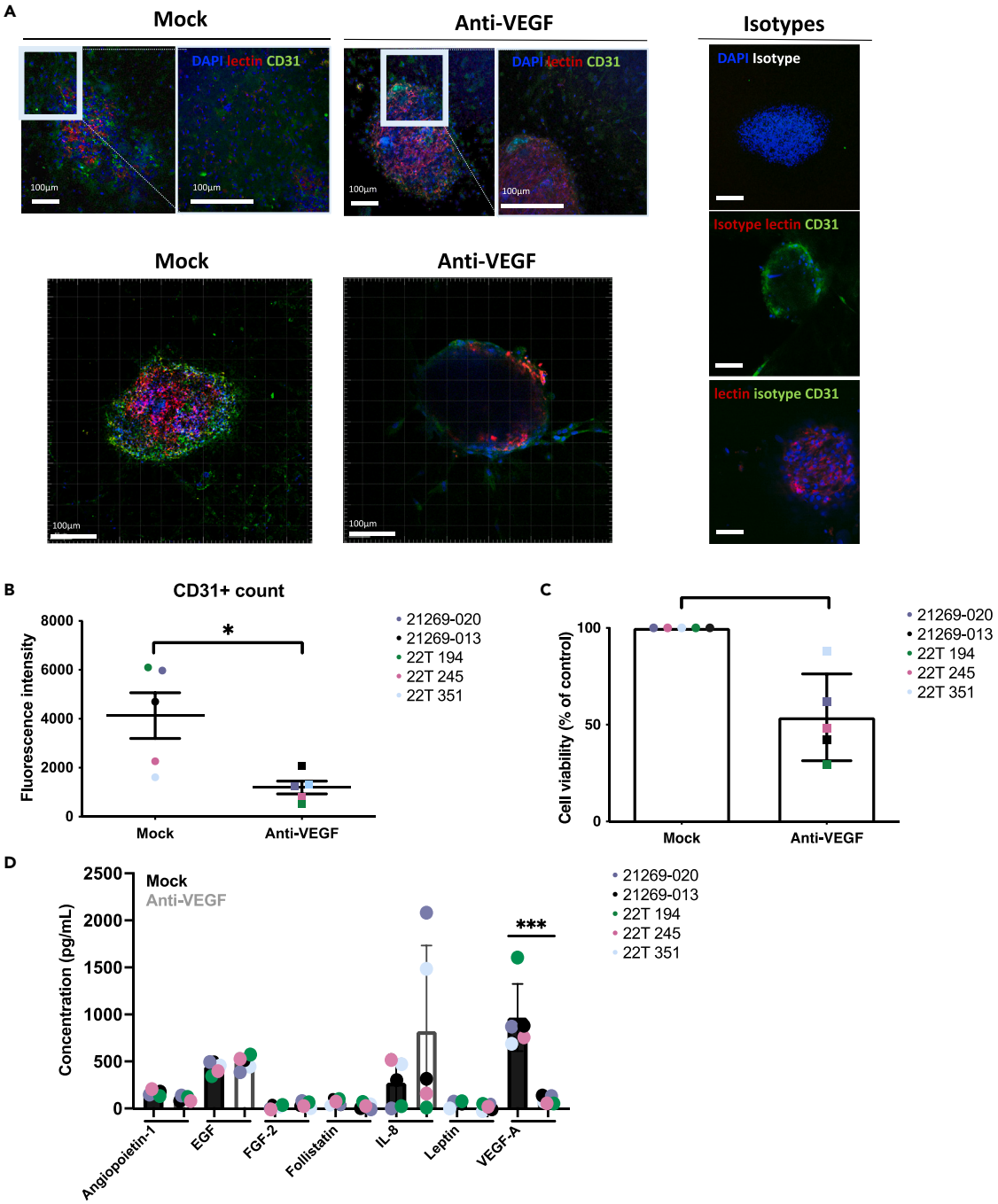

Figure 5. *In vitro* anti-angiogenesis assay provides a tool to study potential antiangiogenic effects

(A) Anti-VEGF was applied on vascularized PDTs embedded in a fibrin gel. After 96 h of treatment, characterization of *de novo* endothelial cells was performed with co-staining of UEA-I lectin and CD31. Matched negative controls and isotypes were also shown. Scale bar: 100µm. Photos below are confocal images that represent a remote view of the structures.

(B) ImageJ was used to count CD31^{+} cells (by fluorescence intensity) that could represent *de novo* structures. Statistics analysis was performed on the 5 patients tested with t test ($p < 0,05$: *).

(C) Cell viability assay of mock and anti-VEGF-treated PDTs (n = 5). Statistics analysis was performed on the 5 patients tested with t test ($p < 0,05$: *).

(D) Graph demonstrated changes in secreted cytokines between mock in black and PDTs treated with anti-VEGF in gray (n = 5). IL-8 and VEGF-A showed significant effect (increase and decrease respectively) ($p < 0,05$ determined by Student t test).

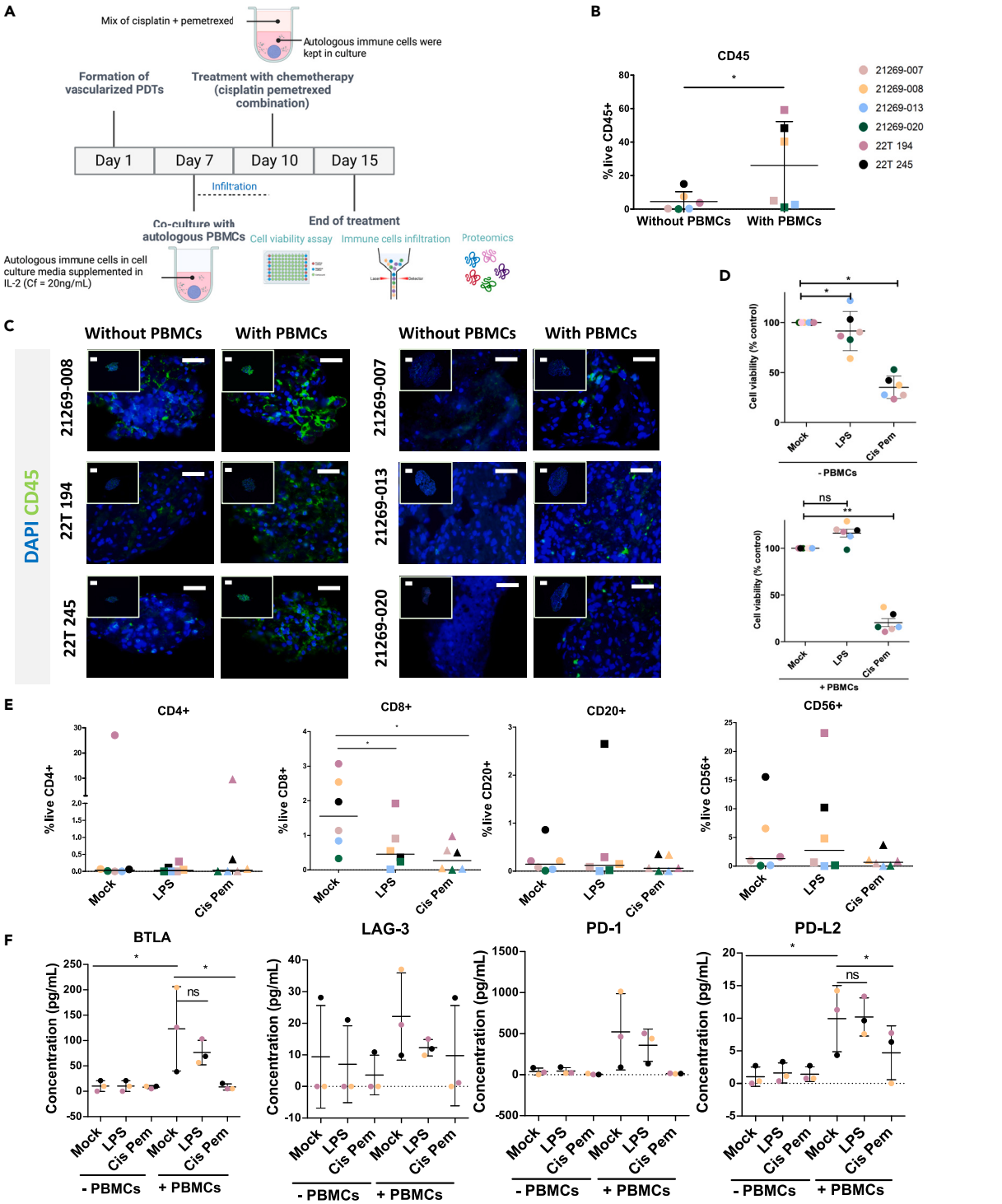

Figure 6. Tri-culture of patients' cells, Ad-MVs, and autologous PBMCs permits to reconstitute a dynamic TME to assess immune effect of chemotherapy

(A) Workflow of the tri-culture. The first seven days of the culture, vascularized PDTs are developing in ULA plates before the tri-culture with autologous PBMCs. IL-2 (cf. = 20 ng/mL) is added in cell culture media to maintain T cells from PBMCs. After 72 h of triculture, chemotherapy treatment is prepared and added in 100µL on top of infiltrated vascularized-PDTs and immune cells that are still in cell culture supernatant. After 96 h of treatment, the endpoint consists of cell viability assay, immune cells infiltration and proteomics studies.

(B) Assessment of immune cells infiltration toward vascularized PDTs by flow cytometry with $CD45^{+}$ marker (n = 6; 21269-007 in light pink, 21269-008 in yellow, 21269-013 in blue, 21269-020 in green, 22T 194 in pink and 22T 245 in black).

Figure 6. *Continued*

(C) Assessment of $CD45^+$ cells by IHC in the conditions without PBMCs or with PBMCs culture. Scale bar: 100 μ m.

(D) Cell viability assessment after 96 h of LPS and chemotherapy treatments without PBMCs and with PBMCs (n = 6).

(E) % of $CD4^+$, $CD8^+$, $CD20^+$, and $CD56^+$ immune cells are checked within PDTs cultured with autologous PBMCs.

(F) Proteins implied in immunosuppression (BTLA, LAG-3, PD-1, and PD-L2) were assessed in PDTs lysates with immuno-oncology panel 1 from Procarta Plex technology in the 3 patients where level of proteins were detectable 21269-008, 22T 194 and 22T 245 (n = 3). Statistics analyses were performed by Student t test (Significantly different ($p < 0.05$)).

See also Figures S4–S8.

Flow cytometry analysis for each patient-derived PBMCs allowed measurement of relative proportions and viability for each subpopulation of sorted cells. It can be noticed that patients' PBMCs profiles were very heterogeneous (See also Figure S6). Culture of PDTs with autologous PBMCs was carried out for at least 72 h in order to allow efficient tumor infiltration (Figure 6A).[63] After having checked the quality of PBMCs, 50,000 PBMCs were added for each PDT and then stimulated with IL-2. After 72 h of culture, the vascularized PDTs were harvested and dissociated for flow cytometry analysis. PDTs were largely infiltrated by functional lymphocytes (Figures 6B and 6C), proportional to initial lymphocyte counts. The three patients, 22T 194, 22T 245, and 21269-008, that displayed higher lymphocyte counts were those with immune-infiltrated PDTs.

On the other hand, patients with low-lymphocyte counts in primary tumoral tissue displayed fewer immune cells within PDTs. Our explanation is that this translates the chemotactic properties of both PBMCs and signaling properties of tumor cells. Our results confirm that vascularized PDTs enrichment, with autologous PBMCs, represents an efficient and reliable approach to the highly dynamic immune infiltration process determining the patient-specific immune cell response.

Assessment of chemotherapy in a reconstituted tumor microenvironment

Combining cisplatin (cis) and pemetrexed (pem) is part of the standard of care treatment for lung cancer patients with no identified driver mutations. It was reported that cisplatin could reactivate the immune cells to favor an antitumor immune response.[64–66] To investigate that, we treated immune-infiltrated vascularized PDTs with cis/pem following the timeline described in Figure 6A.

Cytotoxic effect was monitored with the cell viability assay after 96 h of treatment (i.e., day 15 after the initial surgical resection of the tumor). Lipopolysaccharide (LPS) used as a positive control for activation of infiltrated PBMCs showed no viability decrease (Figure 6D). Cis/pem treatment significantly decreased the viability of PDTs. IFN-γ, a major effector cytokine released by $CD8^+$ T cells, was detected in the supernatant after LPS, not after cis/pem treatment. It is suggested that chemotherapy regimen could have been toxic to $CD8^+$ T cells (See also Figure S7).[67,68]

We then studied the immune cell dynamics of infiltration and migration after 96 h of chemotherapy treatment. The analysis by flow cytometry of immune-infiltrated PDTs confirmed a decrease of $CD8^+$ T cells within PDTs under chemotherapy treatment (Figure 6E). Major pathways of immunosuppression (BTLA, LAG-3, PD-1, and PD-L2) or T cells activation (CD27, CD28, CD80 and CD137) were engaged. Cis/pem regimen largely decreased the expression of BTLA and LAG-3 (Figure 6F), as well as the levels of the four costimulatory molecules involved in T cells activation CD27, CD28, CD80, and CD137 (See also Figure S8). Overall, our data highlighted the impact of chemotherapy on immune cell infiltration and lack of T cell activation.

DISCUSSION

The technology of patient-derived tumoroids has now evolved to the point of constituting an innovative model in oncology, both for drug discovery, and personalized medicine. These tumor avatars can reliably and usefully reproduce *in vitro* patient's specific features. Our vascularized immune-infiltrated PDT model has demonstrated its ability to maintain the morphological, histological, and molecular markers of the primary tumor tissue in culture. It was reported that *ex vivo* growth, culture conditions, and time of culture could influence the formation of PDTs.[69] However, our data, including the very sensitive 3'-RNA sequencing, confirmed that key molecular information for treatment selection had been conserved during the cell culture procedures.

Such a co-culture of Ad-MVs and patient's derived organoids mainly was used in metabolic disease or regenerative medicine.[25,70,71] To our knowledge, this is the first report of the use of a vascularized immune-infiltrated patient-derived model in oncology. A previous study comparing human umbilical vein endothelial cells (HUVECs) with endothelial cells from adipose tissue concluded latter' superiority to form an optimal vascular network.[72] Moreover, α-smooth-muscle-actin (SMA) biomarker was not detected on PDTs cultured with HUVECs, which is a biomarker of vessel maturity.[72] Our experiment analysis confirmed these observations (See also Figure S9). We believe that using other cell types, such as fibroblasts or mesenchymal stem cells[73,74] might broadly alter the transcriptional signature of PDT compared to the primary tumor. Even though Ad-MVs are composed of different cell types, their contribution to providing a stromal tissue environment in the 3D model is well described, particularly for paracrine signals like secreting growth factors and cytokines that help dynamic cell interactions within the PDTs,[48,75] without changing drug response profile.

The next step would be to have a lumenization in the *de novo* structures (in the *in vitro* anti-angiogenesis assay). Longer culture times might improve the formation of complex vasculature structure.[76] Ad-MVs were shown to provide a high-vascularization potential for tumoroids engineering and modeling to model the first steps of angiogenesis *in vitro*.[77] The response to bevacizumab was functionally confirmed to expected effects, i.e., VEGF-A blockade. We could observe an increase in IL-8 for the patients tested. IL-8 is a known proinflammatory signal molecule implied in angiogenesis and tumor growth. IL-8 stimulates tumoral cell proliferation and participates in the recruitment of endothelial cells in the TME.[78] Not surprisingly, anti-VEGF treatment acted directly on the vascular compartment and indirectly on the tumoral mass.

In our model of tri-culture (combining vascularized PDTs and PBMCs), chemotherapy treatment was cytotoxic toward both tumor cells and PBMCs. We observed a reduced release of IFN-γ and a decrease in trafficking and infiltration into the cohesive structure of the vascularized tumoroid. Cis/pem treatment was shown to decrease BTLA, a recently discovered immunosuppressive receptor of the CD28 superfamily with CTLA-4 and PD-L1/PD-1. BTLA interacts with its ligand HVEM leading to downregulation of the immune response by suppressing lymphocyte proliferation.[79] These data suggested that chemotherapy regimen could reverse the immunosuppressive TME. Multiple reports described the depletion of immune cells.[67,68] It might also be that autologous PBMCs only presented naive cells and did not interact with tumor antigens yet. To better investigate the ability of chemotherapy to enhance the antitumor immune response, another solution relies on testing the protocol of tumor-reactive T cells generation from PBMCs described by Cattaneo et al.[31] Another strategy would be to apply the drug prior and then add fresh autologous PBMCs. It was described that chemotherapy could release CXCL chemokines to facilitate immune cell infiltration.[80] Despite the absence of immune cells from the primary tumor, here we demonstrated the feasibility of culturing PDT with autologous immune cells to propose a more relevant 3D model.[14] To keep in culture the tumor resident-immune cells, we will work on adding IL-2 in the cell culture media at the beginning of organoid generation.[81]

This study was the first and essential step to evolve toward a complete autologous model of PDT, wherever tumoral cells could derive from a needle biopsy or surgical resection. Microvessels and lymphocytes derive from a marginal sampling of patient primary tissue, i.e., a small sample of adipose tissue and regular blood sampling, respectively. We demonstrated that our model of PDT comprised the main parts of the TME to apply to immunotherapy or onco-virotherapy. We also showed different sensitivity profiles to both antiangiogenics and chemotherapy within two weeks of culture. A short response time allows saving time for clinicians to have a well-informed therapeutic decision.

Limitations of the study

This study has showed the possibility to vascularize PDTs using Ad-MVs and to perform the *in vitro* anti-angiogenesis assay. One of limitations of this model is the absence of fully perfusable endothelial structures. In future, performing longer culture time might improve the formation of complex vasculature structure to mimic drug delivery.[76] While we observe the infiltration of immune cells in the PDTs, this model couldn't capture the immune-oncogenic activity by infiltrating T cells. This could be improved further by adding cytokines to generate immunogenicity and by maintaining T cells for longer culture periods through the use of pleiotropic agents like IL-2. Another issue is sourcing of the amount of biopsy materials and access to clinical data such as PD-L1 status, anatomopathological profile and long-term patient follow-up to consolidate the *in vitro* observation.

STAR★METHODS

Detailed methods are provided in the online version of this paper and include the following:

- KEY RESOURCES TABLE
- RESOURCE AVAILABILITY
  - Lead contact
  - Materials availability
  - Data and code availability
- EXPERIMENTAL MODEL AND SUBJECT DETAILS
- METHOD DETAILS
  - Human specimens
  - Tissue preparation and co-culture of PDTs and healthy organoids with ad-MVs
  - RNA extraction and integrity
  - 3' RNA sequencing. Pipeline for raw data processing
  - 3' RNA sequencing. Read count normalization and differential gene expression analysis
  - Peripheral Blood Mononuclear cells (PBMCs) isolation
  - *In vitro* anti-angiogenesis assay
  - Culture of PDTs and PBMCs
  - Preparation of drugs
  - Cell Titer Blue Viability Assay
  - Dissociation of PDTs +/- PBMCs for flow cytometry
  - IHC of patients' primary tissues and PDTs
  - Staining of the PDTs embedded by fibrin gel
  - Secretome analysis
  - Protein extraction and quantification
  - Proteomics in cell lysates
  - Flow cytometry acquisition for analyses of PBMCs' subpopulations in PBMCs and dissociated PDTs
- QUANTIFICATION AND STATISTICAL ANALYSIS

SUPPLEMENTAL INFORMATION

Supplemental information can be found online at https://doi.org/10.1016/j.isci.2023.108094.

ACKNOWLEDGMENTS

HL is a recipient of a CIFRE grant from Agence Nationale de la Recherche et de l'Innovation (ANRT, France) to support her PhD work. The authors thank Dr. Joseph Seitlinger, now at CHU Nancy, for initiating the project, Dr. MP Chenard, and the Center de Ressources Biologiques (CRB) department of Strasbourg University Hospital for contribution in sample collection, and management.

The study was conducted in accordance with the Declaration of Helsinki, and approved by Ethics Committee of Grand Est, France (CNRIPH N° 20.11.12.42058). Transgene also acknowledges the European Commission for its support to IMI/imSAVAR (Immune Safety Avatar) consortium (grant agreement n°853988). The various funders had no role in study design, data collection and analysis, decision to publish, or preparation of the manuscript.

AUTHOR CONTRIBUTIONS

This project was conducted by H.-L. and supervised by G.H., J.M.-B., N.B.-J., and E.-Q. The biopsies were provided by surgeons A.O., and P.-E.F. and patients' primary tissue paraffin sections by V.L. C.-P. included all patients and provided patients' clinical data. J.D analyzed the data from transcriptomic part. H.-L. wrote the paper. S.J. participated in data interpretation. S.J., J.-M.B., E.Q., G.H., Y.I.-G., and N.B.-J. participated in the manuscript preparation. All authors have read and agreed to the published version of the manuscript.

DECLARATION OF INTERESTS

C.P., G.H., Y.I.G., V.L., A.O., P.E.F., and N.B.J. declare no competing interests. H.L., J.D., S.J., E.Q., and J.M.B. have been employees, and are shareholders of Transgene S.A. C.Z. was employee of Transgene S.A. at the time of the study design and early experimental studies.

INCLUSION AND DIVERSITY

We support inclusive, diverse, and equitable conduct of research.

Received: June 15, 2023
Revised: August 21, 2023
Accepted: September 26, 2023
Published: September 29, 2023

REFERENCES

1. Sung, H., Ferlay, J., Siegel, R.L., Laversanne, M., Soerjomataram, I., Jemal, A., and Bray, F. (2021). Global Cancer Statistics 2020: GLOBOCAN Estimates of Incidence and Mortality Worldwide for 36 Cancers in 185 Countries. CA. Cancer J. Clin. *71*, 209–249. https://doi.org/10.3322/caac.21660.
2. Denisenko, T.V., Budkevich, I.N., and Zhivotovsky, B. (2018). Cell death-based treatment of lung adenocarcinoma. Cell Death Dis. *9*, 117. https://doi.org/10.1038/s41419-017-0063-y.
3. Zappa, C., and Mousa, S.A. (2016). Non-small cell lung cancer: current treatment and future advances. Transl. Lung Cancer Res. *5*, 288–300. https://doi.org/10.21037/tlcr.2016.06.07.
4. Cancer of the Lung and Bronchus - Cancer Stat Facts SEER. https://seer.cancer.gov/statfacts/html/lungb.html.
5. Ruppert, A.-M., Beau-Faller, M., Debieuvre, D., Ouafik, L., Westeel, V., Rouquette, I., Mazières, J., Bringuier, P.-P., Monnet, I., Escande, F., et al. (2020). Outcomes of Patients With Advanced NSCLC From the Intergroupe Francophone de Cancérologie Thoracique Biomarkers France Study by KRAS Mutation Subtypes. JTO Clin. Res. Rep. *1*, 100052. https://doi.org/10.1016/j.jtocrr.2020.100052.
6. Hou, J., Li, H., Ma, S., He, Z., Yang, S., Hao, L., Zhou, H., Zhang, Z., Han, J., Wang, L., and Wang, Q. (2022). EGFR exon 20 insertion mutations in advanced non-small-cell lung cancer: current status and perspectives. Biomark. Res. *10*, 21. https://doi.org/10.1186/s40364-022-00372-6.
7. Yuan, M., Huang, L.-L., Chen, J.-H., Wu, J., and Xu, Q. (2019). The emerging treatment landscape of targeted therapy in non-small-cell lung cancer. Signal Transduct. Target. Ther. *4*, 61. https://doi.org/10.1038/s41392-019-0099-9.
8. Qu, J., Wang, L., Jiang, M., Zhao, D., Wang, Y., Zhang, F., Li, J., and Zhang, X. (2020). A Review About Pembrolizumab in First-Line Treatment of Advanced NSCLC: Focus on KEYNOTE Studies. Cancer Manag. Res. *12*, 6493–6509. https://doi.org/10.2147/CMAR.S257188.
9. Lee, D., Kim, Y., and Chung, C. (2021). Scientific Validation and Clinical Application of Lung Cancer Organoids. Cells *10*, 3012. https://doi.org/10.3390/cells10113012.
10. Rossi, R., De Angelis, M.L., Xhelili, E., Sette, G., Eramo, A., De Maria, R., Cesta Incani, U., Francescangeli, F., and Zeuner, A. (2022). Lung Cancer Organoids: The Rough Path to Personalized Medicine. Cancers *14*, 3703. https://doi.org/10.3390/cancers14153703.
11. Yokota, E., Iwai, M., Yukawa, T., Yoshida, M., Naomoto, Y., Haisa, M., Monobe, Y., Takigawa, N., Guo, M., Maeda, Y., et al. (2021). Clinical application of a lung cancer organoid (tumoroid) culture system. npj Precis. Oncol. *5*, 29. https://doi.org/10.1038/s41698-021-00166-3.
12. Delom, F., Begiristain, I., Grenier, T., Begueret, H., Soulet, F., Siegfried, G., Khatib, A.-M., Robert, J., and Fessart, D. (2020). Patients Lung Derived Tumoroids (PLDTs) to model therapeutic response. Biochim. Biophys. Acta. Mol. Cell Res. *1867*, 118808. https://doi.org/10.1016/j.bbamcr.2020.118808.
13. Shi, R., Radulovich, N., Ng, C., Liu, N., Notsuda, H., Cabanero, M., Martins-Filho, S.N., Raghavan, V., Li, Q., Mer, A.S., et al. (2020). Organoid Cultures as Preclinical Models of Non–Small Cell Lung Cancer. Clin. Cancer Res. *26*, 1162–1174. https://doi.org/10.1158/1078-0432.CCR-19-1376.
14. Kim, M., Mun, H., Sung, C.O., Cho, E.J., Jeon, H.-J., Chun, S.-M., Jung, D.J., Shin, T.H., Jeong, G.S., Kim, D.K., et al. (2019). Patient-derived lung cancer organoids as *in vitro* cancer models for therapeutic screening. Nat. Commun. *10*, 3991. https://doi.org/10.1038/s41467-019-11867-6.
15. Dijkstra, K.K., Monkhorst, K., Schipper, L.J., Hartemink, K.J., Smit, E.F., Kaing, S., de Groot, R., Wolkers, M.C., Clevers, H., Cuppen, E., and Voest, E.E. (2020). Challenges in Establishing Pure Lung Cancer Organoids Limit Their Utility for Personalized Medicine. Cell Rep. *31*, 107588. https://doi.org/10.1016/j.celrep.2020.107588.
16. Seitlinger, J., Nounsi, A., Idoux-Gillet, Y., Santos Pujol, E., Lê, H., Grandgirard, E., Olland, A., Lindner, V., Zaupa, C., Balloul, J.-M., et al. (2022). Vascularization of Patient-Derived Tumoroid from Non-Small-Cell Lung Cancer and Its Microenvironment. Biomedicines *10*, 1103. https://doi.org/10.3390/biomedicines10051103.
17. Poon, S., and Ailles, L.E. (2022). Modeling the Role of Cancer-Associated Fibroblasts in Tumor Cell Invasion. Cancers *14*, 962. https://doi.org/10.3390/cancers14040962.

18. Sahai, E., Astsaturov, I., Cukierman, E., DeNardo, D.G., Egeblad, M., Evans, R.M., Fearon, D., Greten, F.R., Hingorani, S.R., Hunter, T., et al. (2020). A framework for advancing our understanding of cancer-associated fibroblasts. Nat. Rev. Cancer *20*, 174–186. https://doi.org/10.1038/s41568-019-0238-1.
19. Glabman, R.A., Choyke, P.L., and Sato, N. (2022). Cancer-Associated Fibroblasts: Tumorigenicity and Targeting for Cancer Therapy. Cancers *14*, 3906. https://doi.org/10.3390/cancers14163906.
20. Herrero, A., Knetemann, E., and Mannaerts, I. (2021). Review: Challenges of In Vitro CAF Modelling in Liver Cancers. Cancers *13*, 5914. https://doi.org/10.3390/cancers13235914.
21. Altorki, N.K., Markowitz, G.J., Gao, D., Port, J.L., Saxena, A., Stiles, B., McGraw, T., and Mittal, V. (2019). The lung microenvironment: an important regulator of tumour growth and metastasis. Nat. Rev. Cancer *19*, 9–31. https://doi.org/10.1038/s41568-018-0081-9.
22. Strobel, H.A., Gerton, T., and Hoying, J.B. (2021). Vascularized adipocyte organoid model using isolated human microvessel fragments. Biofabrication *13*, 035022. https://doi.org/10.1088/1758-5090/abe187.
23. Laschke, M.W., Später, T., and Menger, M.D. (2021). Microvascular Fragments: More Than Just Natural Vascularization Units. Trends Biotechnol. *39*, 24–33.
24. Yang, D., Guo, P., He, T., and Powell, C.A. (2021). Role of endothelial cells in tumor microenvironment. Clin. Transl. Med. *11*, e450. https://doi.org/10.1002/ctm2.450.
25. Daum, S., Hagen, H., Naismith, E., Wolf, D., and Pircher, A. (2020). The Role of Anti-angiogenesis in the Treatment Landscape of Non-small Cell Lung Cancer – New Combinational Approaches and Strategies of Neovessel Inhibition. Front. Cell Dev. Biol. *8*, 610903. https://doi.org/10.3389/fcell.2020.610903.
26. Nagl, L., Horvath, L., Pircher, A., and Wolf, D. (2020). Tumor Endothelial Cells (TECs) as Potential Immune Directors of the Tumor Microenvironment – New Findings and Future Perspectives. Front. Cell Dev. Biol. *8*, 766. https://doi.org/10.3389/fcell.2020.00766.
27. Yang, Y., and Schmidt, E.P. (2013). The endothelial glycocalyx: An important regulator of the pulmonary vascular barrier. Tissue Barriers *1*, e23494. https://doi.org/10.4161/tisb.23494.
28. Beyer, S., Blocki, A., Cheung, M.C.Y., Wan, Z.H.Y., Mehrjou, B., and Kamm, R.D. (2021). Lectin Staining of Microvascular Glycocalyx in Microfluidic Cancer Cell Extravasation Assays. Life *11*, 179. https://doi.org/10.3390/life11030179.
29. Yatabe, Y., Dacic, S., Borczuk, A.C., Warth, A., Russell, P.A., Lantuejoul, S., Beasley, M.B., Thunnissen, E., Pelosi, G., Rekhtman, N., et al. (2019). Best Practices Recommendations for Diagnostic Immunohistochemistry in Lung Cancer. J. Thorac. Oncol. *14*, 377–407. https://doi.org/10.1016/j.jtho.2018.12.005.
30. Horimasu, Y., Ishikawa, N., Tanaka, S., Hirano, C., Iwamoto, H., Ohshimo, S., Fujitaka, K., Hamada, H., Hattori, N., and Kohno, N. (2017). MUC1 in lung adenocarcinoma: cross-sectional genetic and serological study. BMC Cancer *17*, 263. https://doi.org/10.1186/s12885-017-3272-y.
31. Nam, M.-W., Kim, C.-W., and Choi, K.-C. (2022). Epithelial-Mesenchymal Transition-Inducing Factors Involved in the Progression of Lung Cancers. Biomol. Ther. *30*, 213–220. https://doi.org/10.4062/biomolther.2021.178.
32. Xiao, D., and He, J. (2010). Epithelial mesenchymal transition and lung cancer. J. Thorac. Dis. *2*, 154–159.
33. Parker, A.L., and Cox, T.R. (2020). The Role of the ECM in Lung Cancer Dormancy and Outgrowth. Front. Oncol. *10*, 1766. https://doi.org/10.3389/fonc.2020.01766.
34. Rokutan-Kurata, M., Yoshizawa, A., Sumiyoshi, S., Sonobe, M., Menju, T., Momose, M., Koyama, M., Shigeto, S., Fujimoto, M., Zhang, M., et al. (2017). Lung Adenocarcinoma With MUC4 Expression Is Associated With Smoking Status, HER2 Protein Expression, and Poor Prognosis: Clinicopathologic Analysis of 338 Cases. Clin. Lung Cancer *18*, e273–e281. https://doi.org/10.1016/j.cllc.2016.11.013.
35. Liang, J., Chen, Z., Huang, Y., Bi, G., Bian, Y., Jin, X., Zhang, H., Sui, Q., Zhan, C., and Wang, Q. (2022). Signatures of malignant cells and novel therapeutic targets revealed by single-cell sequencing in lung adenocarcinoma. Cancer Med. *11*, 2244–2258. https://doi.org/10.1002/cam4.4547.
36. Karantza, V. (2011). Keratins in health and cancer: more than mere epithelial cell markers. Oncogene *30*, 127–138. https://doi.org/10.1038/onc.2010.456.
37. Buccheri, G., and Ferrigno, D. (2001). Lung tumor markers of cytokeratin origin: an overview. Lung Cancer *34* (*Suppl 2*), S65–S69.
38. Chen, Y., Cui, T., Yang, L., Mireskandari, M., Knoesel, T., Zhang, Q., Pacyna-Gengelbach, M., and Petersen, I. (2011). The Diagnostic Value of Cytokeratin 5/6, 14, 17, and 18 Expression in Human Non-Small Cell Lung Cancer. Oncology *80*, 333–340. https://doi.org/10.1159/000329098.
39. Wang, Z., Yang, M.-Q., Lei, L., Fei, L.-R., Zheng, Y.-W., Huang, W.-J., Li, Z.-H., Liu, C.-C., and Xu, H.-T. (2019). Overexpression of KRT17 promotes proliferation and invasion of non-small cell lung cancer and indicates poor prognosis. Cancer Manag. Res. *11*, 7485–7497. https://doi.org/10.2147/CMAR.S218926.
40. Li, C., Teng, Y., Wu, J., Yan, F., Deng, R., Zhu, Y., and Li, X. (2021). A pan-cancer analysis of the oncogenic role of Keratin 17 (KRT17) in human tumors. Transl. Cancer Res. *10*, 4489–4501. https://doi.org/10.21037/tcr-21-2118.
41. Mirhadi, S., Tam, S., Li, Q., Moghal, N., Pham, N.-A., Tong, J., Golbourn, B.J., Krieger, J.R., Taylor, P., Li, M., et al. (2022). Integrative analysis of non-small cell lung cancer patient-derived xenografts identifies distinct proteotypes associated with patient outcomes. Nat. Commun. *13*, 1811. https://doi.org/10.1038/s41467-022-29444-9.
42. Zhan, C., Yan, L., Wang, L., Sun, Y., Wang, X., Lin, Z., Zhang, Y., Shi, Y., Jiang, W., and Wang, Q. (2015). Identification of immunohistochemical markers for distinguishing lung adenocarcinoma from squamous cell carcinoma. J. Thorac. Dis. *7*, 1398–1405.
43. Moin, A.T., Sarkar, B., Ullah, M.A., Araf, Y., Ahmed, N., and Rudra, B. (2021). In silico assessment of EpCAM transcriptional expression and determination of the prognostic biomarker for human lung adenocarcinoma (LUAD) and lung squamous cell carcinoma (LUSC). Biochem. Biophys. Rep. *27*, 101074. https://doi.org/10.1016/j.bbrep.2021.101074.
44. Decary, S., Berne, P.-F., Nicolazzi, C., Lefebvre, A.-M., Dabdoubi, T., Cameron, B., Rival, P., Devaud, C., Prades, C., Bouchard, H., et al. (2020). Preclinical Activity of SAR408701: A Novel Anti-CEACAM5–maytansinoid Antibody–drug Conjugate for the Treatment of CEACAM5-positive Epithelial Tumors. Clin. Cancer Res. *26*, 6589–6599. https://doi.org/10.1158/1078-0432.CCR-19-4051.
45. Ercetin, E., Richtmann, S., Delgado, B.M., Gomez-Mariano, G., Kühnel, J., Korenbaum, E., Liu, B., DeLuca, D., Kühnel, M.P., Jonigk, D., et al. (2019). Clinical Significance of SERPINA1 Gene and Its Encoded Alpha1-antitrypsin Protein in NSCLC. Cancers *11*, 1306. https://doi.org/10.3390/cancers11091306.
46. Chen, W.J., Dong, K.Q., Pan, X.W., Gan, S.S., Xu, D., Chen, J.X., Chen, W.J., Li, W.Y., Wang, Y.Q., Zhou, W., et al. (2023). Single-cell RNA-seq integrated with multi-omics reveals SERPINE2 as a target for metastasis in advanced renal cell carcinoma. Cell Death Dis. *14*, 30. https://doi.org/10.1038/s41419-023-05566-w.
47. Moss, S.M., Schilp, J., Yaakov, M., Cook, M., Schuschke, E., Hanke, B., Strobel, H.A., and Hoying, J.B. (2022). Point-of-use, automated fabrication of a 3D human liver model supplemented with human adipose microvessels. SLAS Discov. *27*, 358–368. https://doi.org/10.1016/j.slasd.2022.06.003.
48. Strobel, H.A., Moss, S.M., and Hoying, J.B. (2023). Vascularized Tissue Organoids. Bioengineering *10*, 124. https://doi.org/10.3390/bioengineering10020124.
49. Arnaoutova, I., and Kleinman, H.K. (2010). In vitro angiogenesis: endothelial cell tube formation on gelled basement membrane extract. Nat. Protoc. *5*, 628–635. https://doi.org/10.1038/nprot.2010.6.
50. Pauty, J., Usuba, R., Cheng, I.G., Hespel, L., Takahashi, H., Kato, K., Kobayashi, M., Nakajima, H., Lee, E., Yger, F., et al. (2018). A Vascular Endothelial Growth Factor-Dependent Sprouting Angiogenesis Assay Based on an In Vitro Human Blood Vessel Model for the Study of Anti-Angiogenic Drugs. EBioMedicine *27*, 225–236. https://doi.org/10.1016/j.ebiom.2017.12.014.
51. Kniebs, C., Luengen, A.E., Guenther, D., Cornelissen, C.G., Schmitz-Rode, T., Jockenhoevel, S., and Thiebes, A.L. (2021). Establishment of a Pre-vascularized 3D Lung Cancer Model in Fibrin Gel—Influence of Hypoxia and Cancer-Specific Therapeutics. Front. Bioeng. Biotechnol. *9*, 761846.
52. Tetzlaff, F., and Fischer, A. (2018). Human Endothelial Cell Spheroid-based Sprouting Angiogenesis Assay in Collagen. Bio. Protoc. *8*, e2995.
53. Brassard-Jollive, N., Monnot, C., Muller, L., and Germain, S. (2020). In vitro 3D Systems to Model Tumor Angiogenesis and Interactions With Stromal Cells. Front. Cell Dev. Biol. *8*, 594903. https://doi.org/10.3389/fcell.2020.594903.
54. Wälchli, T., Bisschop, J., Carmeliet, P., Zadeh, G., Monnier, P.P., De Bock, K., and Radovanovic, I. (2023). Shaping the brain vasculature in development and disease in the single-cell era. Nat. Rev. Neurosci. *24*, 271–298. https://doi.org/10.1038/s41583-023-00684-y.
55. Kempers, L., van der Bijl, I., van Stalborch, A.-M.D., Ponsioen, B., and Margadant, C. (2021). Fast *in vitro* protocol for the visualization and quantitative

high-throughput analysis of sprouting angiogenesis by confocal microscopy. STAR Protoc. *2*, 100690. https://doi.org/10.1016/j.xpro.2021.100690.

56. Russo, A.E., Priolo, D., Antonelli, G., Libra, M., Mccubrey, J.A., and Ferraù, F. (2017). Bevacizumab in the treatment of NSCLC: patient selection and perspectives. Lung Cancer *8*, 259–269. https://doi.org/10.2147/LCTT.S110306.
57. Matsumoto, K., and Ema, M. (2014). Roles of VEGF-A signalling in development, regeneration, and tumours. J. Biochem. (Tokyo) *156*, 1–10. https://doi.org/10.1093/jb/mvu031.
58. Leader, A.M., Grout, J.A., Maier, B.B., Nabet, B.Y., Park, M.D., Tabachnikova, A., Chang, C., Walker, L., Lansky, A., Le Berichel, J., et al. (2021). Single-cell analysis of human non-small cell lung cancer lesions refines tumor classification and patient stratification. Cancer Cell *39*, 1594–1609.e12. https://doi.org/10.1016/j.ccell.2021.10.009.
59. Zilionis, R., Engblom, C., Pfirschke, C., Savova, V., Zemmour, D., Saatcioglu, H.D., Krishnan, I., Maroni, G., Meyerovitz, C.V., Kerwin, C.M., et al. (2019). Single-Cell Transcriptomics of Human and Mouse Lung Cancers Reveals Conserved Myeloid Populations across Individuals and Species. Immunity *50*, 1317–1334.e10. https://doi.org/10.1016/j.immuni.2019.03.009.
60. Yuki, K., Cheng, N., Nakano, M., and Kuo, C.J. (2020). Organoid Models of Tumor Immunology. Trends Immunol. *41*, 652–664. https://doi.org/10.1016/j.it.2020.06.010.
61. Fitzgerald, A.A., Li, E., and Weiner, L.M. (2020). 3D Culture Systems for Exploring Cancer Immunology. Cancers *13*, 56. https://doi.org/10.3390/cancers13010056.
62. Hacker, B.C., and Rafat, M. (2020). Organoids as Complex In Vitro Models for Studying Radiation-Induced Cell Recruitment. Cell. Mol. Bioeng. *13*, 341–357. https://doi.org/10.1007/s12195-020-00625-0.
63. Dijkstra, K.K., Cattaneo, C.M., Weeber, F., Chalabi, M., van de Haar, J., Fanchi, L.F., Slagter, M., van der Velden, D.L., Kaing, S., Kelderman, S., et al. (2018). Generation of Tumor-Reactive T Cells by Co-culture of Peripheral Blood Lymphocytes and Tumor Organoids. Cell *174*, 1586–1598.e12. https://doi.org/10.1016/j.cell.2018.07.009.
64. Merlano, M.C., Denaro, N., Galizia, D., Ruatta, F., Occelli, M., Minei, S., Abbona, A., Paccagnella, M., Ghidini, M., and Garrone, O. (2022). How Chemotherapy Affects the Tumor Immune Microenvironment: A Narrative Review. Biomedicines *10*, 1822. https://doi.org/10.3390/biomedicines10081822.
65. Zhou, Z., Zhao, Y., Chen, S., Cui, G., Fu, W., Li, S., Lin, X., and Hu, H. (2022). Cisplatin Promotes the Efficacy of Immune Checkpoint Inhibitor Therapy by Inducing Ferroptosis and Activating Neutrophils. Front. Pharmacol. *13*, 870178. https://doi.org/10.3389/fphar.2022.870178.
66. Fournel, L., Wu, Z., Stadler, N., Damotte, D., Lococo, F., Boulle, G., Ségal-Bendirdjian, E., Bobbio, A., Icard, P., Trédaniel, J., et al. (2019). Cisplatin increases PD-L1 expression and optimizes immune check-point blockade in non-small cell lung cancer. Cancer Lett. *464*, 5–14. https://doi.org/10.1016/j.canlet.2019.08.005.
67. Lozano-Ojalvo, D., López-Fandiño, R., and López-Expósito, I. (2015). PBMC-Derived T Cells. In The Impact of Food Bioactives on Health: *in vitro* and ex vivo models, K. Verhoeckx, P. Cotter, I. López-Expósito, C. Kleiveland, T. Lea, A. Mackie, T. Requena, D. Swiatecka, and H. Wichers, eds. (Springer International Publishing), pp. 169–180. https://doi.org/10.1007/978-3-319-16104-4_16.
68. Bhat, P., Leggatt, G., Waterhouse, N., and Frazer, I.H. (2017). Interferon-γ derived from cytotoxic lymphocytes directly enhances their motility and cytotoxicity. Cell Death Dis. *8*, e2836. https://doi.org/10.1038/cddis.2017.67.
69. Johnson, K., Anderson, K., Courtois, E., Barthel, F., Varn, F., Luo, D., Yi, E., Kim, H., Estecio, M., Tang, M., et al. EPCO-27. GLIOMA SINGLE CELL MULTI-OMIC ANALYSES REVEALS REGULATORS OF PLASTICITY AND ADAPTIVE STRESS RESPONSE
70. Sun, X., Aghazadeh, Y., and Nunes, S.S. (2022). Isolation of ready-made rat microvessels and its applications in effective *in vivo* vascularization and in angiogenic studies *in vitro*. Nat. Protoc. *17*, 2721–2738. https://doi.org/10.1038/s41596-022-00743-1.
71. Später, T., Marschall, J.E., Brücker, L.K., Nickels, R.M., Metzger, W., Mai, A.-S., Menger, M.D., and Laschke, M.W. (2021). Adipose Tissue-Derived Microvascular Fragments From Male and Female Fat Donors Exhibit a Comparable Vascularization Capacity. Front. Bioeng. Biotechnol. *9*, 777687. https://doi.org/10.3389/fbioe.2021.777687.
72. Freiman, A., Shandalov, Y., Rozenfeld, D., Shor, E., Segal, S., Ben-David, D., Meretzki, S., Egozi, D., and Levenberg, S. (2016). Adipose-derived endothelial and mesenchymal stem cells enhance vascular network formation on three-dimensional constructs *in vitro*. Stem Cell Res. Ther. *7*, 5. https://doi.org/10.1186/s13287-015-0251-6.
73. Kniebs, C., Kreimendahl, F., Köpf, M., Fischer, H., Jockenhoevel, S., and Thiebes, A.L. (2020). Influence of Different Cell Types and Sources on Pre-Vascularisation in Fibrin and Agarose–Collagen Gels. Organogenesis *16*, 14–26. https://doi.org/10.1080/15476278.2019.1697597.
74. Kreimendahl, F., Ossenbrink, S., Köpf, M., Westhofen, M., Schmitz-Rode, T., Fischer, H., Jockenhoevel, S., and Thiebes, A.L. (2019). Combination of vascularization and cilia formation for three-dimensional airway tissue engineering. J. Biomed. Mater. Res. *107*, 2053–2062. https://doi.org/10.1002/jbm.a.36718.
75. Gimble, J.M., Guilak, F., and Bunnell, B.A. (2010). Clinical and preclinical translation of cell-based therapies using adipose tissue-derived cells. Stem Cell Res. Ther. *1*, 19. https://doi.org/10.1186/scrt19.
76. Rautiainen, S., Laaksonen, T., and Koivuniemi, R. (2021). Angiogenic Effects and Crosstalk of Adipose-Derived Mesenchymal Stem/Stromal Cells and Their Extracellular Vesicles with Endothelial Cells. Int. J. Mol. Sci. *22*, 10890. https://doi.org/10.3390/ijms221910890.
77. Später, T., Frueh, F.S., Nickels, R.M., Menger, M.D., and Laschke, M.W. (2018). Prevascularization of collagen-glycosaminoglycan scaffolds: stromal vascular fraction versus adipose tissue-derived microvascular fragments. J. Biol. Eng. *12*, 24. https://doi.org/10.1186/s13036-018-0118-3.
78. Favaro, F., Luciano-Mateo, F., Moreno-Caceres, J., Hernández-Madrigal, M., Both, D., Montironi, C., Püschel, F., Nadal, E., Eldering, E., and Muñoz-Pinedo, C. (2022). TRAIL receptors promote constitutive and inducible IL-8 secretion in non-small cell lung carcinoma. Cell Death Dis. *13*, 1046. https://doi.org/10.1038/s41419-022-05495-0.
79. Li, X., Xu, Z., Cui, G., Yu, L., and Zhang, X. (2020). BTLA Expression in Stage I–III Non–Small-Cell Lung Cancer and Its Correlation with PD-1/PD-L1 and Clinical Outcomes. OncoTargets Ther. *13*, 215–224. https://doi.org/10.2147/OTT.S232234.
80. Opzoomer, J.W., Sosnowska, D., Anstee, J.E., Spicer, J.F., and Arnold, J.N. (2019). Cytotoxic Chemotherapy as an Immune Stimulus: A Molecular Perspective on Turning Up the Immunological Heat on Cancer. Front. Immunol. *10*, 1654.
81. Ross, S.H., and Cantrell, D.A. (2018). Signaling and Function of Interleukin-2 in T Lymphocytes. Annu. Rev. Immunol. *36*, 411–433. https://doi.org/10.1146/annurev-immunol-042617-053352.
82. Köster, J., and Rahmann, S. (2012). Snakemake—a scalable bioinformatics workflow engine. Bioinformatics *28*, 2520–2522. https://doi.org/10.1093/bioinformatics/bts480.
83. Bolger, A.M., Lohse, M., and Usadel, B. (2014). Trimmomatic: a flexible trimmer for Illumina sequence data. Bioinformatics *30*, 2114–2120. https://doi.org/10.1093/bioinformatics/btu170.
84. Smith, R., Ventura, D., and Prince, J.T. (2013). Novel algorithms and the benefits of comparative validation. Bioinformatics *29*, 1583–1585. https://doi.org/10.1093/bioinformatics/btt176.
85. Dobin, A., Davis, C.A., Schlesinger, F., Drenkow, J., Zaleski, C., Jha, S., Batut, P., Chaisson, M., and Gingeras, T.R. (2013). STAR: ultrafast universal RNA-seq aligner. Bioinformatics *29*, 15–21. https://doi.org/10.1093/bioinformatics/bts635.
86. Anders, S., Pyl, P.T., and Huber, W. (2015). HTSeq–a Python framework to work with high-throughput sequencing data. Bioinformatics *31*, 166–169. https://doi.org/10.1093/bioinformatics/btu638.
87. Love, M.I., Huber, W., and Anders, S. (2014). Moderated estimation of fold change and dispersion for RNA-seq data with DESeq2. Genome Biol. *15*, 550. https://doi.org/10.1186/s13059-014-0550-8.
88. Hein, M., and Graver, S. (2013). Tumor cell response to bevacizumab single agent therapy *in vitro*. Cancer Cell Int. *13*, 94. https://doi.org/10.1186/1475-2867-13-94.

STAR★METHODS

KEY RESOURCES TABLE

REAGENT or RESOURCE	SOURCE	IDENTIFIER
Antibodies		
Rabbit anti-TTF-1	Abcam	Cat# ab76013; RRID: AB_1310784
Rabbit anti-Ki-67	LS Bio	Cat# LS-B13463-100
Mouse anti-MUC-1	Novocastra	Cat# NCL-MUC-1-CORE; RRID: AB_564117
Mouse anti-CK-7	Nordic Biosite	Cat# BSH-2018-100
Rabbit lectin-rhodamine	Vector Laboratories	Cat# RL-1062; RRID: AB_2336769
Mouse anti-CD31	Cell Applications	Cat# CB13678
Goat anti-collagen type IV	Merck	Cat# AB769; RRID: AB_92262
Rabbit anti-e-cadherin	Cell Signaling	Cat# 3195; RRID: AB_2291471
Mouse anti-vimentin	DAKO	Cat# M0725; RRID: AB_10013485
Rabbit anti-CD45	Cell Signaling	Cat# 13917S; RRID: AB_2750898
Rabbit anti-α-SMA	Cell Signaling	Cat# 19245; RRID: AB_2734735
Anti-CD45 V450	BD Biosciences	Cat# 560367; RRID: AB_1645573
Anti-CD3 AF700	Biolegend	Cat# 317340; RRID: AB_2563408
Anti-CD14 V500	BD Biosciences	Cat# 561391; RRID: AB_10611856
Anti-CD16 FITC	BD Biosciences	Cat# 335035; RRID: AB_2868680
Anti-HLA DR APC Cy7	Biolegend	Cat# 307618; RRID: AB_493587
Anti-CD4 PE	BD Pharmingen	Cat# 555347; RRID: AB_395752
Anti-CD8 BV650	Biolegend	Cat# 301042; RRID: AB_11125174
Anti-CD20 PE Cy7	Miltenyi	Cat# 130-111-340; RRID: AB_2656074
Anti-CD56 PE Cy7	Miltenyi	Cat# 130-113-313; RRID: AB_2726091
Anti-CD11c PE Cy5	Biolegend	Cat# 301610; RRID: AB_493578
Biological samples		
Human tumor tissue samples	This study	N/A
Human peri-tumoral tissue samples	This study	N/A
Human blood samples	This study	N/A
Adipocytes-derived microvessels (Ad-MVs)	Advanced Solutions®, Manchester NH, USA	https://www.advancedsolutions.com/microvessels
Chemicals, peptides, and recombinant proteins		
PBS	Sigma	Cat#W3500
DMEM-F12	Gibco	Cat#12634028
Amphotericin B	Gibco	Cat#15290026
Penicillin-Streptomycin	Sigma	Cat# V900929
Collagenase I	Worthington biochemical	Cat#LS004217
DNAse I	Worthington biochemical	Cat#LS002138
Elastase	Worthington biochemical	Cat#LS002290
Hyaluronidase	Worthington biochemical	Cat#LS002594
RPMI 1640	Thermofisher Scientific	Cat#11879020
Foetal Bovine Serum (FBS)	Gibco	Cat#10099141
Gentamycin	Sigma	Cat#G1272
B-27	Thermofisher Scientific	Cat#17504044
Human-recombinant VEGF-165	Thermofisher Scientific	Cat#PHC9394

(*Continued on next page*)

Continued

REAGENT or RESOURCE	SOURCE	IDENTIFIER
DMEM high glucose	Gibco	Cat#41966-029
Ficoll Paque Plus reagent	Cytiva	Cat#17144003
DMSO	Sigma	Cat#2650
FGF-2	Merck	Cat#01-106
EGF	Sigma	Cat#E5036
HGF	Sigma	Cat#SRP60-14-10mg
Fibrinogen	Sigma	Cat#F3879-1G
Thrombin	Sigma	Cat#T6884-1KU
IL-2	Miltenyi	Cat#130-097-744
Bevacizumab	Selleckchem	Cat#A2006
Cisplatin	Merck	Cat#232150-50mg
Pemetrexed	Sigma	Cat#SML1490-50mg
Accutase	StemPro	Cat#A1110501
Histogel	Thermofisher Scientific	Cat#HG-4000-012
H2O2	Sigma	Cat#H1009
Goat serum	Sigma	Cat#G6767
Bovine Serum Albumin (BSA)	Sigma	Cat#A9647
DAPI	Sigma	Cat#B2883
Triton X-100	Sigma	Cat#T-8787
RIPA lysis buffer	Thermofisher Scientific	Cat#89901
Phosstop	Roche	Cat#04 906 837 001
cOmplete tablets	Roche	Cat#4693116001
Live/dead reagent	Invitrogen	Cat#L34955
Lipopolysaccharide (LPS)	Escherichia Coli 0127:B8 Merck	Cat#L3129-10mg
Critical commercial assays		
RNA extraction kit	Qiagen	Cat#74134
Agilent RNA 6000 Nano Kit	Agilent Technologies	Cat#5067-1511
Cell Titer Blue	Promega	Cat#G8081
Bond Primary Antibody Diluent	Leica	Cat#AR9590
Bond Wash solution 10X	Leica	Cat#AR9590
Post-Primary/ Novolink reagents	Leica	Cat#7161
Tyramide Signal Amplification (TSA)	Perkin Elmer	Cat#SAT701B
DC protein assay kit	Bio-Rad	Cat#500-0116
18-plex angiogenesis kit	Invitrogen	Cat# EPX180-15806-901
IFN-γ ELISA kit	Invitrogen	Cat#KHC4021
14-plex immuno-oncology checkpoints kit	Invitrogen	Cat#EPX14A-15803-901
Deposited data		
3'RNA sequencing	This paper	GEO: GSE240662
Experimental models: Organisms/strains		
Human lung tumoroids and healthy organoid samples	This study	N/A
Software and algorithms		
GraphPad Prism	Version 9.0	https://www.graphpad.com

(*Continued on next page*)

Continued

REAGENT or RESOURCE	SOURCE	IDENTIFIER
Other		
Fluorescence microscope	Nikon	Eclipse 90i
Confocal microscope	Zeiss	LSM Zeiss 800
HistoCore PEARL tissue processor	Leica	https://www.leicabiosystems.com/fr-fr/equipement-dhistologie/traitement-des-tissus/histocore-pearl/
BOND-MAX automated stainer	Leica	https://www.leicabiosystems.com/fr-fr/ihc-ish/coloration-avancee-ihc-ish/bond-max-fully-automated-ihc-and-ish-casino/

RESOURCE AVAILABILITY

Lead contact

Further information and requests for resources and reagents should be directed to and will be fulfilled by the Lead Contact, Lê Hélène (lhelene@live.fr).

Materials availability

This study did not generate new unique reagents.

Data and code availability

- 3′ RNA-seq data have been deposited at GEO and are publicly available as of the date of publication, under the accession number GSE240662. Microscopy data reported in this paper will be shared by the lead contact upon request.
- This paper does not report the original code.
- Any additional information required to reanalyze the data reported in this paper is available from the lead contact upon request.

EXPERIMENTAL MODEL AND SUBJECT DETAILS

Primary tumor and peritumoral tissues were obtained from NSCLC patients who underwent major lung resection for localized lung cancer in the Thoracic Surgery Department of Strasbourg University Hospital. They were aged 18 years or older, and their written informed consent was obtained the day before the surgery. As soon as the lung resection was performed, a 5 mm by 5 mm fragment was taken by an anatomopathologist without interfering with the clinical pathological diagnosis. This study was conducted in accordance with the Declaration of Helsinki, and approved by the Ethics Committee of Grand Est, France (CNRIPH n° 20.11.12.42058).

Clinical information is available in Table S1.

METHOD DETAILS

Human specimens

Samples of lung cancer were obtained by surgical resections at Hôpitaux Universitaires de Strasbourg, France, (6 patients) confirmed for their tumoral status by anatomopathological analysis. Healthy lung tissue samples were also obtained from lung parenchyma from the tumor of matched patients. Patients' informed consents were managed by the *Centre de Ressources Biologiques* (CRB). Adenocarcinoma tissue samples paired with autologous whole blood were sourced from CRB, Strasbourg and Fidelis Research, Bulgaria. Ad-MVs were isolated from human subcutaneous adipose tissue and stored in liquid nitrogen by Advanced solutions®, Manchester NH, USA. Ad-MVs constitute the basis of their human vascularization platform for the generation of 3D tissue and organoids, either *in vivo* or *in vitro*. These cell types can undergo angiogenesis under induction to provide an intact microvasculature within 3D system, according to the supplier.

Tissue preparation and co-culture of PDTs and healthy organoids with ad-MVs

After reception, human samples were washed in PBS to remove blood excess, then enzymatically digested at 37°C and 5° CO_2 for 1 hr, with intermittent agitation (300 rpm). The enzymatic mix is composed of 20 mL of digestion medium (DMEM/F12 (ref. 12634028, Gibco), 0.4% amphotericin B (ref. 15290026, Gibco), 1% penicillin-streptomycin (ref. V900929, Sigma), 500 µg/mL collagenase I (ref. LS004217, Worthington biochemical), 25 µg/mL DNAse I (ref. LS002138, Worthington biochemical), 25 µg/mL elastase (ref. LS002290, Worthington biochemical), 100 µg/mL hyaluronidase (ref. LS002594, Worthington biochemical)). The media was then transferred to a Falcon tube through 70 µm cell strainers. Strained cells were centrifuged, and pellets were resuspended in 1 mL of lysis buffer (Ammonium-Chlorure-Potassium (ACK)) buffer composed of 0.1 mM EDTA, 150 mM NH4Cl, 10 mM KHCO3) to remove remaining blood cells. A second centrifugation was performed, and

the left cells were resuspended in 1 mL DMEM-F12 (ref. 12634028, Gibco). Other cells entering the composition of PDTs were prepared in parallel. For the formation of tumoroids and organoids, cultured with ad-MVs, after the tissue preparation described previously, cells from Advanced Solutions were thawed in the water bath then centrifuged at 400g during 4min. The ad-MVs pellet is then resuspended in RPMI media (ref. 11879020, Thermofisher Scientific) supplemented with 10% fetal bovine serum (FBS) (ref. 10099141, Gibco), 1% gentamycin (ref. G1272, Sigma), B-27 (ref. 17504044, ThermoFisher Scientific, Cf = 1X) and human-recombinant VEGF (ref. PHC9394, ThermoFisher Scientific, C_f = 50ng/mL). We used the concentration of B27 and VEGF that were described by the supplier. Ad-MVs and patients' dissociated cells were mixed (5000 patient derived cells from either tumor sample or healthy tissue and 5000 Ad-MVs per organoid) in cell culture medium. As we mixed two different cell types, the cell culture media was composed of 50% of RPMI medium + 50% of DMEM/F12 supplemented with 10% FBS, 1% gentamycin, B27 1X and 50ng/mL VEGF) in each well of a 96-well U-bottom Ultra-low attachment (ULA) plate (ref. S-bio, Tokyo Japan, or ref. Thermofisher Nunclon Sphera-treated). PDTs and healthy organoids are usually formed in a 3D shape after 7 days of incubation at 37°C, 5° CO_2. On day 3 of the culture, the media is changed to fresh media. This fresh media contains DMEM high glucose (ref. 41966-029, Gibco) instead of DMEM-F12 which is usually used for seeding steps. Regarding the supplementary data Figure S9 describing the co-culture of patients' cells with HUVECs, HUVECs (Cat. C-003-5C) were split at low passage (P3-4). HUVECs and patients' dissociated cells were mixed (5000 patient derived cells from tumor sample and 5000 HUVECs per organoid) in cell culture medium. For this co-culture, the cell culture media was composed of 50% endothelial cell culture media (ref. PB BH 100 9806, Pelo Biotech) + 50% DMEM-F12 supplemented with 10% FBS, 1% gentamycin and supplements from the endothelial cell culture.

RNA extraction and integrity

Prior to RNA extraction, organoids were pooled and washed in PBS before freezing at -80°C. Upon thawing, the lysis buffer from the Qiagen kit was added to the Eppendorf. This is then transferred to a Miltenyi M-tube (ref. 130-096-335, Miltenyi) and lysis is performed using the RNA extraction_01 program. A 1 min centrifugation at 1000rpm is performed before proceeding with the rest of the protocol from the supplier Qiagen (ref. 74134, Qiagen).

RNA amounts are assayed with Nanodrop and RNA integrity is also checked on Agilent chips (ref. 5067-1511, Agilent Technologies). Prior processing RNA samples, 50 ng of total RNA per sample were prepared. One sample per condition was processed to 3'RNA sequencing, performed by Integragen.

3' RNA sequencing. Pipeline for raw data processing

Raw paired reads generated by high-throughput sequencing were first processed using a bioinformatic pipeline developed with the tool Snakemake.[82] Briefly, 3 extra G added during library preparation were removed from read 2 using trimmomatic.[83] Then, the Unique Molecular Identifier (UMI) sequence was extracted from read 1 and appended to the name of the paired read 2 (extract function from the UMI-tools package.[84] Read 2 from each pair were then mapped against the reference genome (GRCh37) with STAR.[85] Reads mapped at a given position of the genome with identical or near identical UMI sequence were deduplicated with the program umi_tools dedup, using the method "directional." Readcount per cellular gene was then determined with the program htseq-count, mode "union".[86]

3' RNA sequencing. Read count normalization and differential gene expression analysis

To account for potential differences in sequencing depth between samples, the read count was normalized with DESeq2.[87] A gene was considered differentially expressed comparing two conditions if the adjusted p value (Benjamini and Hochberg method) was £ 0.1 and the absolute fold change 2^3.

To assess the ability of the organoid model to recapitulate the transcriptomic signatures seen in primary tumor cells, log2 fold change (l2FC) of mRNA steady-state level for primary tumor cells versus primary healthy cells was plotted (x-axis) against log2 fold-change for patient derived tumoroid versus healthy organoid (y axis). The Pearson correlation coefficient was calculated for each of the three patients independently.

Peripheral Blood Mononuclear cells (PBMCs) isolation

Autologous blood sample was delivered with tumoral tissue by CRB and Fidelis Research. Firstly, blood was diluted with an equal volume of PBS and mixed slowly. A falcon with Ficoll Paque Plus reagent (ref. 17144003, Cytiva) was prepared and diluted blood was carefully overlayed to begin density gradient separation. Centrifugation was performed with the break off (350g during 25 min). The PBMC layer was carefully collected in another falcon. Once the density gradient separation was done, three washing steps were performed to remove the contaminants as described in the following step. PBS was added to the collected PBMCs, and centrifugation was performed without the break off (350g during 8 min). After PBS washing steps, lysis buffer was added to remove the remaining blood cells (ref. R7757, Sigma). Then, centrifugation was performed, and the cell pellet was resuspended in PBS. After PBMC isolation, PBMC were cryopreserved in 10% DMSO (ref. 2650, Sigma), 20% FBS diluted in RPMI media, and stored at -80°C. Addition of PBMCs to PDTs was performed at day 7 and the infiltration was left for at least 72 hrs according previous methods.[63] Timeline was created by BioRender (AN25ETXK99).

In vitro anti-angiogenesis assay

On day 7 of the culture, inserts were prepared the day of the PDTs transfer. Fibrin gel is pipetted into cell culture inserts (ref. Thincert 665 610 Greiner Bio-One) that are placed in the 12 wells plate. Preparation of fibrin gel is described in a previous article by mixing fibrinogen (ref. F3879-1G, Sigma, C_f = 5mg/mL), VEGF (ref. PHC9394, ThermoFisher Scientific, C_f = 500ng/mL) and thrombin (ref. T6884-1KU, Sigma, C_f = 4UI/mL).[16] The inserts were then transferred in the incubator for at least 30 min, then, 600 µL of RPMI media supplemented with VEGF (C_f = 50 ng/mL, ref. PHC9394, ThermoFisher Scientific), FGF-2 (C_f = 20ng/mL, ref. 01-106, Merck), EGF (C_f = 100 ng/mL, ref. E5036-500mg, Sigma), HGF (C_f = 30 ng/mL, ref. SRP60-14-10 mg, Merck) and B27 (C_f = 1X, ref. 17504044, ThermoFisher Scientific) were added in the 12 wells plate. After 30 min of incubation at 37°C, the formed tumoroids were laid on the fibrin gel for at least 24 h to observe the migration of endothelial tip cells.

Culture of PDTs and PBMCs

On day 7 of the culture, PBMCs were thawed and counted to start with the culture. PBMCs were cultured with tumoral organoids at the ratio of 50,000 PBMCs for 1 organoid. To maintain T cells and help their proliferation, IL-2 was added in the RPMI media at final concentrations of 20 ng/mL (ref. 130-097-744, Miltenyi).

Preparation of drugs

Bevacizumab (ref. A2006, Selleckchem). The dose used for *in vitro* testing of bevacizumab was 250µg/mL according to Hein&Graver.[88] The drug was diluted in cell culture media and applied on fibrin gel containing tumoroids for 96 h.

LPS from Escherichia Coli 0127:B8 (ref. L3129-10mg, Merck). The final concentration used was 10mg/mL, diluted in DMEM cell culture media.

Chemotherapy (cisplatin ref. 232150-50mg, Merck & pemetrexed ref. SML1490-50mg, Sigma). Cisplatin and pemetrexed stock solutions at 1 mM and 1.296 mM, respectively, were prepared and reconstituted in DMEM culture medium (ref. 41966-029, Gibco). Final concentrations of cisplatin and pemetrexed used were 9 and 24 µM, respectively in 100 µL/well of the ULA plate. The PDTs were treated with chemotherapy for 96 hrs at 37°C, 5% CO_2.

Cell Titer Blue Viability Assay

The viability of tumoroids was assessed with the CellTiter-Blue Cell Viability Assay (ref. G8081, Promega). This is a fluorimetric assay based on resazurin reduction. When the drug treatment is stopped, the CellTiter-Blue Cell Viability Assay is incubated with the organoids for 24 h at 37°C. (The CellTiter-Blue Cell Viability Assay is previously prepared according to the supplier''s recommendations). After 24 hrs, the medium is transferred to a 96-well plate with a transparent flat bottom. Using a luminometer (TECAN M1000), the fluorescence at (560Ex/590Em) was measured. Viability tests were conducted on 6 organoids per condition and viability normalized to the untreated control (Mock).

Dissociation of PDTs +/- PBMCs for flow cytometry

After either 72 hrs of co-culture and chemotherapy treatments, PDTs were priorly washed in PBS and pooled in a 1,5mL tube. PBS was removed and 300mL of Accutase (ref. A1110501, StemPro Accutase) was added. Up to ten resuspensions are done with low-binding tips, then, the Eppendorfs were incubated at 37°C with permanent agitation during five to ten minutes. PDTs were dissociated into single cell culture and staining protocol for flow cytometry acquisition were performed.

IHC of patients' primary tissues and PDTs

PDTs were fixed in 4% PFA and embedded in Histogel specimen processing gel (ref. HG-4000-012, ThermoFisher Scientific) before dehydration in the HistoCore PEARL. After paraffin inclusion, the blocks were sectioned on the Leica microtome at the size of 5µm. Then, immunohistochemistry (IHC) and standard hematoxylin and eosin (H&E) staining were performed on these sectioned slides. IHC staining was performed on the LEICA Bond-MAX system using the tyramid signal amplification (TSA) method. The first steps of IHC are the dewaxing and the antigen unmasking (either High pH buffer or citrate buffer during 20min). Saturation of endogenous peroxydases with 10min of incubation in 3% H2O2 (ref. H1009, Sigma) and blocking step with goat serum for 30min (ref. G6767, Sigma) were performed. For collagen type IV (the specie host is goat), we used 1% BSA (ref. A9647, Sigma). The following primary antibodies were prepared in Bond Primary Antibody Diluent (AR9590, Leica) : anti-TTF-1 (dilution 1:250; ref. ab76013, Abcam), anti-Ki-67 (dilution 1:5000; ref. LS-B13463-100, LS bio), anti-MUC-1 (dilution 1:200; ref. NCL-MUC-1-CORE, Novocastra), and anti-CK-7 (dilution 1:300; ref. BSH-2018-100, Nordic BioSite), lectin (dilution 1:100; ref. UEA-1 lectin Vector Laboratories RL-1062), anti-CD-31 (dilution 1:250, ref. CB13678, Cell Applications), anti-collagen type IV (dilution 1:20; ref. AB769, Merck), anti-e-cadherin (dilution 1:400; ref. 3195, Cell Signaling), anti-vimentin (dilution 1:1000; ref. M0725, DAKO), anti-CD45 (dilution 1:250; ref. 13917S, Cell Signaling) and anti-α-SMA (dilution 1:100; ref. 19245 Cell Signaling). They were incubated for 1 hr at room temperature (RT). The value of dilution is based on the concentration of the antibody in the stock solution and the concentration used. After 1 hr of incubation with the primary antibody, secondary antibodies (or post-primary which is a rabbit anti-mouse IgG) and tertiary antibody (Novolink-polymer which is an anti-rabbit Poly-HRP) were incubated during 30 min at RT sequentially (ref. 7161, Leica). The post-primary was applied for primary mouse antibodies only. The final step was the signal amplification based on TSA using Perkin Elmer kit (ref. SAT701B, Perkin Elmer), for 10min at RT. Cell nuclei were stained with DAPI (dilution 1:10000 in PBS; ref. B2883, Sigma) during 10min at RT. The washing steps were performed

between each step with Bond wash solution 1X (ref. AR9590, Leica). H&E staining was performed on paraffin sections that were prior deparaffinized in xylene and different solutions of ethanol. Coloration with hematoxylin and eosin solutions was done followed by dehydration with ethanol 100% and xylene. Images were taken on the fluorescence microscopy Nikon Eclipse 90i.

Staining of the PDTs embedded by fibrin gel

After 24 hrs in fibrin gel, the PDTs embedded by fibrin gel were prior fixed with 4% PFA overnight at 4°C. 0,25% Triton X solution (ref. T-8787, Sigma) was added for 30 min at RT. 1% BSA blocking buffer (ref. A9647, Sigma) was then added for 4 hrs at RT. Lectin staining (dilution 1:100; ref. UEA-1 lectin Vector Laboratories RL-1062) was performed for 24 hrs. The stained PDTs and gels were washed at least 4 times with PBS at 30min of interval (one washing was overnight at 4°C). Then anti-CD31 (dilution 1:250; ref. CB13678, Cell Applications) was prepared and let for 72 hrs of incubation at 4°C. Secondary antibody directed against the primary antibody was incubated for 24 hrs at 4°C (dilution 1:200; ref. A32723, Invitrogen). Finally, DAPI solution (dilution 1:3000 in distilled water; ref. B-2883, Sigma) was added for one hour at RT. PBS washing was done before acquisition in LSM Zeiss 800 confocal microscopy. Z-stack images were captured using 1mm slice (with approximatively 60-70 XY images) and presented as maximum z-projections. Image analysis in 3D view and orthogonal projections in XY, XZ, YZ were done on the Imaris software. Quantification of $CD31^+$ cells was performed using NIH Image J.

For acquisition on the light-sheet microscopy, samples were sent fixed and stained to IMACTIV-3D, Toulouse. The workflow was created with BioRender (LU25ETXLXP).

Secretome analysis

Cytokines and interleukines analyzed were CD31 (PECAM-1), EGF, FGF-2, G-CSF, HGF, IL-8, Leptin, PDGF-BB, Syndecan, VEGF-A, VEGF-D, Angiopoietin-1, BMP-9, EMMPRIN, Follistatin, HB-EGF, LYVE-1 and TIE-2. These cytokines and interleukines were designed by Procarta Plex with the Human Angiogenesis panel 18-plex (ref. EPX180-15806-901, Invitrogen). For quantification of IFN-γ in the supernatant, the IFN-γ human ELISA kit (ref. KHC4021, Invitrogen) was used according to the supplier protocol.

Protein extraction and quantification

Organoids from the same condition were pooled (6 in number) in an Eppendorf and rinsed with PBS. The PBS was removed, and the organoids were frozen at -80°C before extraction. RIPA lysis buffer (ref. 89901, ThermoScientific) supplemented with Phosstop (ref. 04 906 837 001, Roche) and cOmplete tablets (ref. 4693116001, Roche) was used to lyse the organoids under sonication to perform protein extraction. The amount of protein was quantified using the DC protein assay kit (ref. 500-0116, Bio-Rad) according to the supplier's recommendations.

Proteomics in cell lysates

For experiments relative to culture with PBMCs, cytokines and interleukines analyzed were CD27, CD28, CD137 (4-1BB), GITR, HVEM, BTLA, CD80, CD152 (CTLA-4), IDO, LAG-3, PD-1, PD-L1, PD-L2 and TIM-3. These cytokines and interleukines were designed by Procarta Plex with the Human Immuno-oncology panel I 14-plex (ref. EPX14A-15803-901, Invitrogen). The protocol was drawn according to the manufacturer's indications. Only detectable cytokines were shown in this article.

Flow cytometry acquisition for analyses of PBMCs' subpopulations in PBMCs and dissociated PDTs

Following the thawing of PBMCs, PBMCs subpopulation were investigated with cell surface markers staining. The PBMCs subpopulations were studied with this panel: Live/dead FVS575V (dilution 1:1000; ref. L34955, Invitrogen), anti-CD45 V450 (ref. 560367, BD Biosciences), anti-CD3 AF700 (ref. 317340, Biolegend), anti-CD14 V500 (ref. 561391, BD Biosciences), anti-CD16 FITC (ref. 335035, BD Biosciences), anti-HLA DR APC Cy7 (ref. 307618, Biolegend), anti-CD4 PE (ref. 555347, BD Pharmingen), anti-CD8 BV650 (ref. 301042, Biolegend), anti-CD20 PE Cy7 (ref. 130-111-340, Miltenyi), anti-CD56 PE Cy7 (ref. 130-113-313, Miltenyi) and anti-CD11c PE Cy5 (ref. 301610, Biolegend). Incubation with Live/Dead reagent and antibodies was for 30 min at 4°C in the darkness. After 30 min of incubation, cells were centrifuged at 350g during 8 min at 4°C and resuspended in 100µL of PBS before acquisition on the MACSQuant 16 (Miltenyi Germany).

QUANTIFICATION AND STATISTICAL ANALYSIS

Data was analyzed using GraphPad Prism 9. The statistical method used was a paired two-tailed Student''s t-test to determine cell viability of antiangiogenic, and chemotherapy treatments based on the ratio of the resorufin fluorescence signal of treated PDTs to that of untreated (or mock) PDTs on day 4 after treatment. This t-test was also used to compare changes in proteins under antiangiogenic, and chemotherapy treatments to that of untreated (or mock). n represents the number of patients used for each assay and a significance threshold of $p<0,05$ was used to determine a significant effect of a treatment.